with HCV infection. Nicola A. Fletcher reported that brain microvascular endothelial cells express all the recognized entry factors for HCV, and brain microvascular endothelial cells actually support infection by HCVpp and HCVcc. This suggests potential disorders of the central nervous system in HCV infection.

Treatment

In the keynote lecture, Masashi Mizokami presented "Genome-wide association study and its application for HCV treatment." He emphasized that the functional relevance of IL-28B single nucleotide polymorphisms should be elucidated to further advance the progress of research on the mechanisms of chronic HCV infection and treatment.

Yasuhiro Asahina presented that genetic variation in IL-28B is associated with gene expression involving innate immunity. Minor alleles of IL-28B, as well as a higher RIG-I/IPS-1 ratio are associated with null viral response. Martin Laggins correlated IL-28B genetic variation with pretreatment levels of IP-10 and HCV RNA throughout therapy. The favorable genetic variation of IL-28B single nucleotide polymorphisms (major allele) was significantly associated with lower baseline IP-10. Masao Honda revealed that hepatic IFN-stimulated genes (ISGs) are associated with genetic variation in IL-28B and the outcome of IFN therapy for chronic hepatitis C using microarray gene expression profiling of the biopsied liver samples. Multivariate logistic regression analysis showed that ISGs, fibrosis stage, and ISDR mutations were strongly associated with viral response. Hepatic ISGs were associated with the IL-28B polymorphism and expression was significantly higher in patients with the minor genotype than in those with the major genotype. Takashi Motomura also analyzed ISG expression using liver transplantation samples. Expression of ISGs in recipients' liver carrying the minor allele of IL-28B was significantly up-regulated when compared with the major allele. Surprisingly, IFN sensitivity for recurrent hepatitis C after liver transplantation is influenced by IL-28B genetic variation not only in recipients, but also in donors.

Drug Development

This session opened with a keynote lecture by Raffaele De Francesco describing the current state of drug development for patients with chronic hepatitis C. Because of the rapid development of NS3/4A, NS5A, and NS5B inhibitors, he finally presented the hopeful message "Will there be an HCV meeting in 2020?".

Lotte Coelmont characterized an NS5A D320E variant showing low-level resistance to DEB025, a cyclophilin (Cyp)-binding molecule. This study suggests that DEB025 presents a high barrier to resistance, and that D320E confers low-level resistance to DEB025 by reducing the need for CypA-dependent isomerization of NS5A. Paul Targett-Adams reported that NS5A inhibitors stimulated redistribution of NS5A from the ER to ring-like structures in the cytoplasm, and disrupted colocalization with NS5B. This study suggests that NS5A inhibitors perturb formation of new replication complexes rather than acting on preformed complexes. Luis M. Schang developed a family of small synthetic rigid amphiphiles with large hydrophilic heads and small, planar and rigid hydrophobic tails, called RAFIs (rigid amphipathic fusion inhibitors), which inhibit the infectivity of enveloped virions including HCV. Emmanuel Thomas screened host genes involving the anti-HCV activity of ribavirin. Among 64 host genes, several candidate genes were identified as host factors involving ribavirin's anti-HCV activity. Interestingly, silencing of the *ITPA* gene increased the anti-HCV activity of ribavirin. Pablo Gastaminza identified a novel family of 1,2-diamines as an anti-HCV reagent from a chemical library. The analysis of ~300 derivatives identified several compounds with enhanced potency and low cytotoxicity.

Vaccines/Epidemiology

HCV therapeutic vaccines are aimed to induce effective T-cell responses. Marianne Mikkelsen reported that vaccination of mice with recombinant adenovirus expressing HCV NS3 fused to the MHC class II chaperon protein invariant chain significantly enhanced NS3 specific $CD8^+$ T-cell responses, and protected mice against NS3-expressing vaccinia virus challenge. This vaccination induced polyfunctional $CD8^+$ memory T cells. Lars Frelin aimed to restore immunologic function through vaccination in a transgenic mouse model with impaired HCV-specific T-cell responses owing to a persistent presence of hepatic HCV NS3/4A antigens. They found that heterologous sequences improved activation and expansion of NS3/4A-specific T cells in a wild-type host, as well as in a tolerant NS3/4A-transgenic mouse model. The authors also suggested an important role for Tregs in the impaired HCV-specific T-cell responses.

Livia M.G. Rossi examined antibody cross-immunoreactivity against different HVR1 variants to identify antigens with a possible application of HCV vaccine development. The authors identified a small set of HVR1 variants that cross-immunoreacted with a large number of HVR1 peptides, thus suggesting their potential use in the development of HCV vaccine candidates.

Conclusion

HCV2010 in Yokohama was successful and contributed to the progress of research in the field. HCV infection remains one of the most serious worldwide health problems. The goals of this symposium were to

increase the scientific understanding of this virus and gain insights applicable to future efforts to control its infection. From this point of view, we gained further fundamental understanding about HCV at the meeting. The discovery of IL-28B as a new host factor involved in HCV treatment and pathogenesis had a major impact on HCV research. New treatment advances have been made in recent years and will continue in the near future. We would like to conclude that this meeting was successful in providing opportunities for exchanging up-to-date information and international collaboration. The next meeting will take place in Seattle, Washington, from September 8–12, 2011 (http://www.hcv2011.org/).

Reprint requests

Address requests for reprints to: Takaji Wakita, MD, PhD, Department of Virology II, National Institute of Infectious Diseases, 1-23-1 Toyama, Shinjuku-ku, Tokyo 162-8640, Japan. e-mail: wakita@nih.go.jp; fax 81-3-5285-1161.

Conflicts of interest

The authors disclose no conflicts.

JOURNAL OF VIROLOGY, July 2011, p. 6882–6892 Vol. 85, No. 14
0022-538X/11/$12.00 doi:10.1128/JVI.02418-10

Hepatitis C Virus Hijacks P-Body and Stress Granule Components around Lipid Droplets[▽]

Yasuo Ariumi,[1,2]* Misao Kuroki,[1] Yukihiro Kushima,[3] Kanae Osugi,[4] Makoto Hijikata,[3] Masatoshi Maki,[4] Masanori Ikeda,[1] and Nobuyuki Kato[1]

Department of Tumor Virology, Okayama University Graduate School of Medicine, Dentistry, and Pharmaceutical Sciences, Okayama 700-8558, Japan[1]; Center for AIDS Research, Kumamoto University, Kumamoto 860-0811, Japan[2]; Department of Viral Oncology, Institute for Virus Research, Kyoto University, Kyoto 606-8507, Japan[3]; and Department of Applied Molecular Biosciences, Graduate School of Bioagricultural Sciences, Nagoya University, Nagoya 464-8601, Japan[4]

Received 19 November 2010/Accepted 21 April 2011

The microRNA miR-122 and DDX6/Rck/p54, a microRNA effector, have been implicated in hepatitis C virus (HCV) replication. In this study, we demonstrated for the first time that HCV-JFH1 infection disrupted processing (P)-body formation of the microRNA effectors DDX6, Lsm1, Xrn1, PATL1, and Ago2, but not the decapping enzyme DCP2, and dynamically redistributed these microRNA effectors to the HCV production factory around lipid droplets in HuH-7-derived RSc cells. Notably, HCV-JFH1 infection also redistributed the stress granule components GTPase-activating protein (SH3 domain)-binding protein 1 (G3BP1), ataxin-2 (ATX2), and poly(A)-binding protein 1 (PABP1) to the HCV production factory. In this regard, we found that the P-body formation of DDX6 began to be disrupted at 36 h postinfection. Consistently, G3BP1 transiently formed stress granules at 36 h postinfection. We then observed the ringlike formation of DDX6 or G3BP1 and colocalization with HCV core after 48 h postinfection, suggesting that the disruption of P-body formation and the hijacking of P-body and stress granule components occur at a late step of HCV infection. Furthermore, HCV infection could suppress stress granule formation in response to heat shock or treatment with arsenite. Importantly, we demonstrate that the accumulation of HCV RNA was significantly suppressed in DDX6, Lsm1, ATX2, and PABP1 knockdown cells after the inoculation of HCV-JFH1, suggesting that the P-body and the stress granule components are required for the HCV life cycle. Altogether, HCV seems to hijack the P-body and the stress granule components for HCV replication.

Hepatitis C virus (HCV) is the causative agent of chronic hepatitis, which progresses to liver cirrhosis and hepatocellular carcinoma. HCV is an enveloped virus with a positive single-stranded 9.6-kb RNA genome, which encodes a large polyprotein precursor of approximately 3,000 amino acid (aa) residues. This polyprotein is cleaved by a combination of the host and viral proteases into at least 10 proteins in the following order: core, envelope 1 (E1), E2, p7, nonstructural 2 (NS2), NS3, NS4A, NS4B, NS5A, and NS5B (12, 13, 21). The HCV core protein, a nucleocapsid, is targeted to lipid droplets (LDs), and the dimerization of the core protein by a disulfide bond is essential for the production of infectious virus (24). Recently, LDs have been found to be involved in an important cytoplasmic organelle for HCV production (26). Budding is an essential step in the life cycle of enveloped viruses. The endosomal sorting complex required for transport (ESCRT) system has been involved in such enveloped virus budding machineries, including that of HCV (5).

DEAD-box RNA helicases with ATP-dependent RNA-unwinding activities have been implicated in various RNA metabolic processes, including transcription, translation, RNA splicing, RNA transport, and RNA degradation (32). Previously, DDX3 was identified as an HCV core-interacting protein by yeast two-hybrid screening (25, 29, 43). Indeed, DDX3 is required for HCV RNA replication (3, 31). DDX6 (Rck/p54) is also required for HCV replication (16, 33). DDX6 interacts with an initiation factor, eukaryotic initiation factor 4E (eIF-4E), to repress the translational activity of mRNP (38). Furthermore, DDX6 regulates the activity of the decapping enzymes DCP1 and DCP2 and interacts directly with Argonaute-1 (Ago1) and Ago2 in the microRNA (miRNA)-induced silencing complex (miRISC) and is involved in RNA silencing. DDX6 localizes predominantly in the discrete cytoplasmic foci termed the processing (P) body. Thus, the P body seems to be an aggregate of translationally repressed mRNPs associated with the translation repression and mRNA decay machinery.

In addition to the P body, eukaryotic cells contain another type of RNA granule termed the stress granule (SG) (1, 6, 22, 30). SGs are aggregates of untranslating mRNAs in conjunction with a subset of translation initiation factors (eIF4E, eIF3, eIF4A, eIFG, and poly(A)-binding protein [PABP]), the 40S ribosomal subunits, and several RNA-binding proteins, including PABP, T cell intracellular antigen 1 (TIA-1), TIA-1-related protein (TIAR), and GTPase-activating protein (SH3 domain)-binding protein 1 (G3BP1). SGs regulate mRNA translation and decay as well as proteins involved in various aspects of mRNA metabolisms. SGs are cytoplasmic phase-dense structures that occur in eukaryotic cells exposed to various environmental stress, including heat, arsenite, viral infection, oxidative conditions, UV irradiation, and hypoxia. Impor-

* Corresponding author. Mailing address: Center for AIDS Research, Kumamoto University, 2-2-1 Honjo, Kumamoto 860-0811, Japan. Phone and fax: 81 96 373 6834. E-mail: ariumi@kumamoto-u.ac.jp.
▽ Published ahead of print on 4 May 2011.

tantly, several viruses target SGs and stress granule components for viral replication (10, 11, 34, 39). Recent studies suggest that SGs and the P body physically interact and that mRNAs may move between the two compartments (1, 6, 22, 28, 30).

miRNAs are a class of small noncoding RNA molecules ~21 to 22 nucleotides (nt) in length. miRNAs usually interact with 3′-untranslated regions (UTRs) of target mRNAs, leading to the downregulation of mRNA expression. Notably, the liver-specific and abundant miR-122 interacts with the 5′-UTR of the HCV RNA genome and facilitates HCV replication (15, 17, 19, 20, 31). Ago2 is at least required for the efficient miR-122 regulation of HCV RNA accumulation and translation (40). However, the molecular mechanism(s) for how DDX6 and miR-122 as well as DDX3 positively regulate HCV replication is not fully understood. Therefore, we investigated the potential role of P-body and stress granule components in HCV replication.

MATERIALS AND METHODS

Cell culture. 293FT cells were cultured in Dulbecco's modified Eagle's medium (DMEM; Invitrogen, Carlsbad, CA) supplemented with 10% fetal bovine serum (FBS). HuH-7-derived RSc cured cells, in which cell culture-generated HCV-JFH1 (JFH1 strain of genotype 2a) (37) could infect and effectively replicate, were cultured in DMEM with 10% FBS as described previously (3–5, 23).

Plasmid construction. To construct pcDNA3-FLAG-DDX6, a DNA fragment encoding DDX6 was amplified from total RNAs derived from RSc cells by reverse transcription (RT)-PCR using KOD-Plus DNA polymerase (Toyobo) and the following pairs of primers: 5′-CGGGATCCAAGATGAGCACGGCC AGAACAGAGAACCCTGTT-3′ (forward) and 5′-CCGCTCGAGTTAAGGT TTCTCATCTTCTACAGGCTCGCT-3′ (reverse). The obtained DNA fragments were subcloned into either BamHI-XhoI site of the pcDNA3-FLAG vector (2), and the nucleotide sequences were determined by BigDye termination cycle sequencing using an ABI Prism 310 genetic analyzer (Applied Biosystems, Foster City, CA).

RNA interference. The following small interfering RNAs (siRNAs) were used: human ATXN2/ATX2/ataxin-2 (siGENOME SMRT pool M-011772-01-005), human PABP1/PABPC1 (siGENOME SMRT pool M-019598-01-005), human Lsm1 (siGENOME SMRT pool M-005124-01-005), human Xrn1 (siGENOME SMRT pool M-013754-01-005), human G3BP1 (ON-TARGETplus SMRT pool L-012099-00-005), human PATL1 (siGENOME SMRT pool M-015591-00-005), and siGENOME nontargeting siRNA pool 1 (D-001206-13-05) (Dharmacon, Thermo Fisher Scientific, Waltham, MA), as a control. siRNAs (25 nM final concentration) were transiently transfected into RSc cells (3–5, 23) using Oligofectamine (Invitrogen) according to the manufacturer's instructions. Oligonucleotides with the following sense and antisense sequences were used for the cloning of short hairpin RNA (shRNA)-encoding sequences targeted to DDX6 (DDX6i) as well as the control nontargeting shRNA (shCon) in a lentiviral vector: 5′-GATCC CCGGAGGAACTAACTCTGAAGTTCAAGAGACTTCAGAGTTAGTTCCT CCTTTTTGGAAA-3′ (sense) and 5′-AGCTTTTCCAAAAAGGAGGAACTAA CTCTGAAGTCTCTTGAACTTCAGAGTTAGTTCCTCCGGG-3′ (antisense) for DDX6i and 5′-GATCCCCGAATCCAGAGGTAATCTACTTCAAGAGA GTAGATTACCTCTGGATTCTTTTTGGAAA-3′ (sense) and 5′-AGCTTTTC CAAAAAGAATCCAGAGGTAATCTACTCTCTTGAAGTAGATTACCTC TGGATTCGGG-3′ (antisense) for shCon. The oligonucleotides described above were annealed and subcloned into the BglII-HindIII site, downstream from an RNA polymerase III promoter of pSUPER (8), to generate pSUPER-DDX6i and pSUPER-shCon, respectively. To construct pLV-DDX6i and pLV-shCon, the BamHI-SalI fragments of the corresponding pSUPER plasmids were subcloned into the BamHI-SalI site of pRDI292, an HIV-1-derived self-inactivating lentiviral vector containing a puromycin resistance marker allowing for the selection of transduced cells (7). pLV-DDX3i, described previously (3), was used.

Lentiviral vector production. The vesicular stomatitis virus G protein (VSV-G)-pseudotyped HIV-1-based vector system was described previously (27, 44). The lentiviral vector particles were produced by the transient transfection of the second-generation packaging construct pCMV-ΔR8.91 (27, 44), the VSV-G-envelope-expressing plasmid pMDG2, as well as pRDI292 into 293FT cells with FuGene6 reagent (Roche Diagnostics, Mannheim, Germany).

HCV infection experiments. The supernatants were collected from cell culture-generated HCV-JFH1 (37)-infected RSc cells (3–5, 23) at 5 days postinfection and stored at −80°C after filtering through a 0.45-μm filter (Kurabo, Osaka, Japan) until use. For infection experiments with HCV-JFH1, RSc cells (1×10^5 cells/well) were plated onto 6-well plates and cultured for 24 h. We then infected the cells at a multiplicity of infection (MOI) of 1 or 4. The culture supernatants were collected at 24 h postinfection, and the levels of the core protein were determined by an enzyme-linked immunosorbent assay (ELISA) (Mitsubishi Kagaku Bio-Clinical Laboratories, Tokyo, Japan). Total RNA was also isolated from the infected cellular lysates by using an RNeasy minikit (Qiagen, Hilden, Germany) for analysis of intracellular HCV RNA. The infectivity of HCV-JFH1 in the culture supernatants was determined by a focus-forming assay at 48 h postinfection. HCV-JFH1-infected cells were detected by using anti-HCV core (CP-9 and CP-11 mixture).

Quantitative RT-PCR analysis. The quantitative RT-PCR analysis of HCV RNA was performed by real-time LightCycler PCR (Roche) as described previously (3–5, 14, 23). We used the following forward and reverse primer sets for the real-time LightCycler PCR: 5′-ATGAGTCATGTGGCAGTGGA-3′ (forward) and 5′-GCTGGCTGTACTTCCTCCAC-3′ (reverse) for DDX3, 5′-ATG AGCACGGCCAGAACAGA-3′ (forward) and 5′-TTGCTGTGTCTGTGTGC CCC-3′ (reverse) for DDX6, 5′-TGACGGGGTCACCCACACTG-3′ (forward) and 5′-AAGCTGTAGCCGCGCTCGGT-3′ (reverse) for β-actin, and 5′-AGA GCCATAGTGGTCTGCGG-3′ (forward) and 5′-CTTTCGCAACCCAACGC TAC-3′ (reverse) for HCV-JFH1.

Preparation of anti-PATL1 antibody. The anti-PATL1 antiserum was raised in rabbits using the glutathione *S*-transferase (GST)-fused PATL1 Ct (C-terminal region of PATL1, aa 450 to 770) as an antigen, and immunoglobulins were affinity purified by using the maltose-binding protein (MBP)-fused PATL1 Ct that was immobilized on an *N*-hydroxysuccinimide (NHS) column (GE Healthcare Bio-Sciences AB, Uppsala, Sweden).

Preparation of LDs. Lipid droplets (LDs) were prepared as described previously (26). Cells were pelleted by centrifugation at 1,500 rpm. The pellet was resuspended in hypotonic buffer (50 mM HEPES [pH 7.4], 1 mM EDTA, 2 mM $MgCl_2$) supplemented with a protease inhibitor cocktail (Nacalai Tesque, Kyoto, Japan) and was incubated for 10 min at 4°C. The suspension was homogenized with 30 strokes of a glass Dounce homogenizer using a tight-fitting pestle (Wheaton, Millville, NJ). A 1/10 volume of 10× isotonic buffer {0.2 M HEPES (pH 7.4), 1.2 M potassium acetate (KoAc), 40 mM magnesium acetate [$Mg(oAc)_2$], and 50 mM dithiothreitol (DTT)} was added to the homogenate. The nuclei were removed by centrifugation at 2,000 rpm for 10 min at 4°C. The supernatant was collected and centrifuged at 16,000 × *g* for 10 min at 4°C. The supernatant was mixed with an equal volume of 1.04 M sucrose in isotonic buffer (50 mM HEPES, 100 mM KCl, 2 mM $MgCl_2$, and protease inhibitor cocktail). The solution was set in a 13.2-ml Polyallomer centrifuge tube (Beckman Coulter, Brea, CA). One milliliter of isotonic buffer was loaded onto the sucrose mixture. The tube was centrifuged at 100,000 × *g* in an SW41Ti rotor (Beckman Coulter) for 1 h at 4°C. After the centrifugation, the LD fraction on the top of the gradient solution was recovered in phosphate-buffered saline (PBS). The collected LD fraction was used for Western blot analysis.

Western blot analysis. Cells were lysed in a buffer containing 50 mM Tris-HCl (pH 8.0), 150 mM NaCl, 4 mM EDTA, 1% Nonidet P-40, 0.1% sodium dodecyl sulfate (SDS), 1 mM DTT, and 1 mM phenylmethylsulfonyl fluoride. Supernatants from these lysates were subjected to SDS-polyacrylamide gel electrophoresis, followed by immunoblot analysis using anti-DDX3 (catalog no. 54257 [NT] and 5428 [IN]; Anaspec, San Jose, CA), anti-DDX6 (A300-460A; Bethyl Laboratories, Montgomery, TX), anti-adipose differentiation-related protein (ADFP; GTX110204; GeneTex, San Antonio, TX), anti-calnexin (NT; Stressgen, Ann Arbor, MI), anti-HCV core (CP-9 and CP-11; Institute of Immunology, Tokyo, Japan), anti-β-actin antibody (A5441; Sigma, St. Louis, MO), anti-ATX2/SCA2 antibody (A302-033A; Bethyl), anti-PABP (sc-32318 [10E10]; Santa Cruz Biotechnology, Santa Cruz, CA), anti-PABP (ab21060; Abcam, Cambridge, United Kingdom), anti-G3BP1 (611126; BD Transduction Laboratories, San Jose, CA), anti-LSM1 (LS-C97364, Life Span Biosciences, Seattle, WA), anti-HSP70 (610607; BD), anti-XRN1 (A300-443A; Bethyl), or anti-PATL1 antibody.

Immunofluorescence and confocal microscopic analysis. Cells were fixed in 3.6% formaldehyde in PBS, permeabilized in 0.1% NP-40 in PBS at room temperature, and incubated with anti-DDX3 antibody (54257 [NT] and 5428 [IN]; Anaspec), anti-DDX3X (LS-C64576; Life Span), anti-DDX6 (A300-460A; Bethyl), anti-HCV core (CP-9 and CP-11), anti-ATX2/SCA2 antibody (A302-033A; Bethyl), anti-ataxin-2 (611378; BD), anti-PABP (ab21060; Abcam), anti-G3BP1 (A302-033A; Bethyl), anti-LSM1 (LS-C97364; Life Span), anti-XRN1

(A300-443A; Bethyl), anti-Dcp2 (A302-597A; Bethyl), anti-human Ago2 (011-22033; Wako, Osaka, Japan), or anti-PATL1 antibody at a 1:300 dilution in PBS containing 3% bovine serum albumin (BSA) for 30 min at 37°C. The cells were then stained with fluorescein isothiocyanate (FITC)-conjugated anti-rabbit antibody (Jackson ImmunoResearch, West Grove, PA) at a 1:300 dilution in PBS containing BSA for 30 min at 37°C. Lipid droplets and nuclei were stained with borondipyrromethene (BODIPY) 493/503 (Molecular Probes, Invitrogen) and DAPI (4′,6-diamidino-2-phenylindole), respectively, for 15 min at room temperature. Following extensive washing in PBS, the cells were mounted onto slides using a mounting medium of 90% glycerin–10% PBS with 0.01% *p*-phenylenediamine added to reduce fading. Samples were viewed under a confocal laser scanning microscope (LSM510; Zeiss, Jena, Germany).

Statistical analysis. A statistical comparison of the infectivities of HCV in the culture supernatants between the knockdown cells and the control cells was performed by using the Student *t* test. *P* values of less than 0.05 were considered statistically significant. All error bars indicate standard deviations.

RESULTS

HCV infection hijacks the P-body components. To investigate the potential role of P-body components in the HCV life cycle, we first examined the alteration of the subcellular localization of DDX3 or DDX6 by HCV-JFH1 infection using confocal laser scanning microscopy as previously described (2), since both DDX3 and DDX6 were identified previously as P-body components (6). For this, we used HuH-7-derived RSc cells, in which cell culture-generated HCV-JFH1 (JFH1 strain of genotype 2a) (37) can infect and effectively replicate (3, 4, 23). HCV-JFH1-infected RSc cells at 60 h postinfection were stained with anti-HCV core antibody, anti-DDX3, and/or anti-DDX6. Lipid droplets (LDs) and nuclei were stained with BODIPY 493/503 and DAPI (4′,6-diamidino-2-phenylindole), respectively. Samples were viewed under a confocal laser scanning microscope. Although we observed that endogenous DDX3 localized in faint cytoplasmic foci in uninfected RSc cells, DDX3 relocalized, formed ringlike structures, and colocalized with the HCV core protein in response to HCV-JFH1 infection (Fig. 1A). On the other hand, endogenous DDX6 was localized in the evident cytoplasmic foci termed P bodies in the uninfected cells (Fig. 1A). DDX6 also relocalized, formed ringlike structures, and colocalized with the core protein in response to HCV-JFH1 infection (Fig. 1A). Although we failed to observe that most of the P bodies of DDX6 perfectly colocalized with DDX3 in uninfected RSc cells (Fig. 1B), we observed a few P bodies of DDX6 colocalized with DDX3 in the uninfected cells (Fig. 1B, arrowheads). Intriguingly, we found that endogenous DDX3 colocalized with endogenous DDX6 in HCV-JFH1-infected cells (Fig. 1B). To further confirm this finding, pHA-DDX3 (41) and pcDNA3-FLAG-DDX6 were cotransfected into 293FT cells. Consequently, we observed that hemagglutinin (HA)-DDX3 colocalized with FLAG-DDX6 in 293FT cells coexpressing HA-DDX3 and FLAG-DDX6 (Fig. 1B), suggesting cross talk of DDX3 with DDX6. Recently, LDs have been found to be involved in an important cytoplasmic organelle for HCV production (26). Indeed, both DDX3 and DDX6 were recruited around LDs in response to HCV infection, while these proteins did not colocalize with LDs in uninfected naïve RSc cells (Fig. 1C). Furthermore, both DDX3 and DDX6 accumulated in the LD fraction of the HCV-JFH1-infected RSc cells; however, we could not detect both proteins in the LD fraction from uninfected control cells (Fig. 1D), suggesting that DDX3 and DDX6 are recruited around LDs in response to HCV infection.

These results suggest that HCV-JFH1 infection disrupts P-body formation. Therefore, we further examined whether or not HCV-JFH1 disrupts the P-body formations of other microRNA effectors, including Ago2; the Sm-like protein Lsm1, which is a subunit of heptameric-ring Lsm1-7, involved in decapping; the 5′-to-3′ exonuclease Xrn1; the decapping activator PATL1; and the decapping enzyme DCP2 (6, 21, 30). As expected, HCV-JFH1 disrupted the P-body formations of Ago2, Lsm1, and Xrn1 as well as PATL1 (Fig. 2). Lsm1, Xrn1, or PATL1 relocalized, formed ringlike structures, and colocalized with the HCV core protein in response to HCV-JFH1 infection, whereas they were localized predominantly in P bodies in uninfected RSc cells (Fig. 2). In fact, we observed that DDX6 colocalized with Ago2, a P-body marker (Fig. 2). In contrast, HCV-JFH1 failed to disrupt the P-body formation of DCP2 (Fig. 2). Thus, these results suggest that HCV disrupts P-body formation through the hijacking of P-body components.

HCV hijacks stress granule components. Since Nonhoff et al. recently reported that DDX6 interacted with ataxin-2 (ATX2) (28), we examined the potential cross talk among DDX6, ATX2, and HCV. Although ATX2 and G3BP1, a well-known stress granule component (36), were dispersed in the cytoplasm at 37°C, both proteins formed discrete aggregates termed stress granules and colocalized with each other in response to heat shock at 43°C for 45 min, indicating that ATX2 is also stress granule component (Fig. 3A). We did not observe prominent colocalization between DDX6 and ATX2 at 37°C (Fig. 3B). In contrast, we found that DDX6 was recruited, juxtaposed, and partially colocalized with stress granules of ATX2 in response to heat shock at 43°C for 45 min in the uninfected RSc cells (Fig. 3B). Notably, ATX2 was recruited, formed the ring-like structures, and partially colocalized with DDX6 in response to HCV-JFH1 infection even at 37°C (Fig. 3B). Furthermore, we noticed that ATX2 was recruited around LDs in HCV-JFH1-infected cells at 72 h postinfection, while ATX2 did not colocalize with LDs in uninfected cells (Fig. 3C), suggesting the colocalization of ATX2 with the HCV core protein in infected cells. Indeed, ATX2 colocalized with the HCV core protein in HCV-JFH1-infected RSc cells at 37°C (Fig. 3D). Moreover, HCV-JFH1 infection induced the colocalization of the core protein with other stress granule components, G3BP1 or PABP1 as well as ATX2 (Fig. 4 and 5). To further confirm our findings, we examined the time course of the redistribution of DDX6 and G3BP1 after inoculation with HCV-JFH1. Consequently, we still detected the P-body formation of DDX6 and dispersed G3BP1 in the cytoplasm, and we did not observe a colocalization between the HCV core protein and DDX6 at 12 and 24 h postinfection (Fig. 4). In contrast, we found that the P-body formation of DDX6 began to be disrupted at 36 h postinfection (Fig. 4). Consistently, G3BP1 formed stress granules at 36 h postinfection (Fig. 4). We then noticed a ringlike formation of DDX6 or G3BP1 and colocalization with the HCV core protein after 48 h postinfection (Fig. 4), suggesting that the disruption of P-body formation and the hijacking of P-body and stress granule components occur in a late step of HCV infection.

We then examined whether or not HCV-JFH1 infection

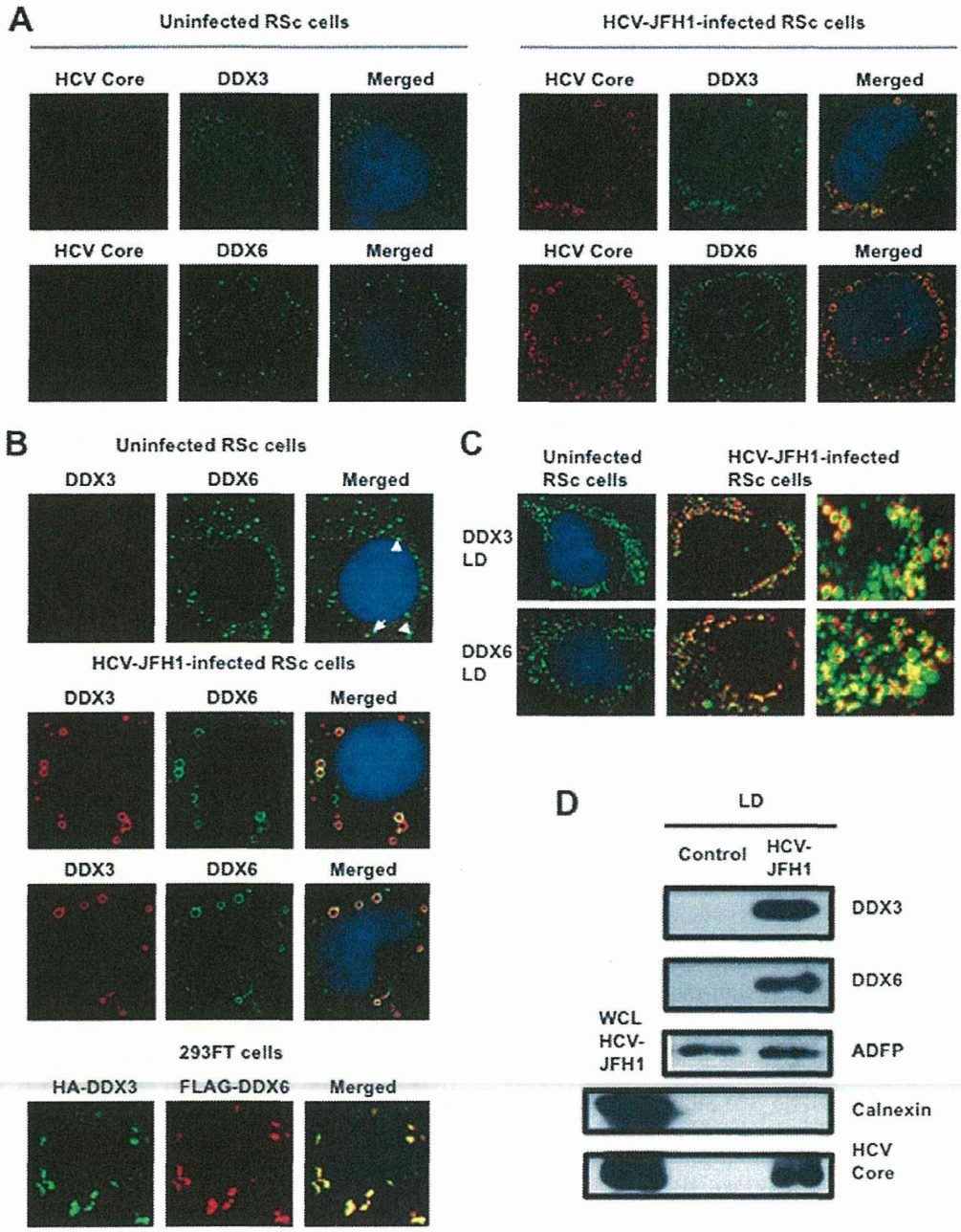

FIG. 1. Dynamic recruitment of DDX3 and DDX6 around lipid droplets (LDs) in response to HCV-JFH1 infection. (A) HCV-JFH1 disrupts the P-body formation of DDX6. Cells were fixed at 60 h postinfection and were then examined by confocal laser scanning microscopy. Cells were stained with anti-HCV core (CP-9 and CP-11 mixture) and either anti-DDX3 (54257 and 54258 mixture) or anti-DDX6 (A300-460A) antibody and then visualized with FITC (DDX3 or DDX6) or Cy3 (core). Images were visualized by using confocal laser scanning microscopy. The two-color overlay images are also exhibited (merged). Colocalization is shown in yellow. (B) HCV-JFH1 recruits DDX3 or DDX6 around LDs. Cells were stained with either anti-DDX3 or anti-DDX6 antibody and were then visualized with Cy3 (red). Lipid droplets and nuclei were stained with BODIPY 493/503 (green) and DAPI (blue), respectively. A high-magnification image is also shown. (C) Colocalization of DDX3 with DDX6. HCV-JFH1-infected RSc cells at 60 h postinfection were stained with anti-DDX3X (LS-C64576) and anti-DDX6 (A300-460A) antibodies. 293FT cells cotransfected with 100 ng of pcDNA3-FLAG-DDX6 and 100 ng of pHA-DDX3 (41) were stained with anti-FLAG-Cy3 and anti-HA-FITC antibodies (Sigma). (D) Association of DDX3 and DDX6 with LDs in response to HCV-JFH1 infection. The LD fraction and whole-cell lysates (WCL) were collected from uninfected RSc cells (control) or HCV-JFH1-infected RSc cells at 5 days postinfection. The results of Western blot analyses of DDX3, DDX6, and the HCV core protein as well as the LD marker ADFP and the endoplasmic reticulum (ER) marker calnexin in the LD fraction are shown.

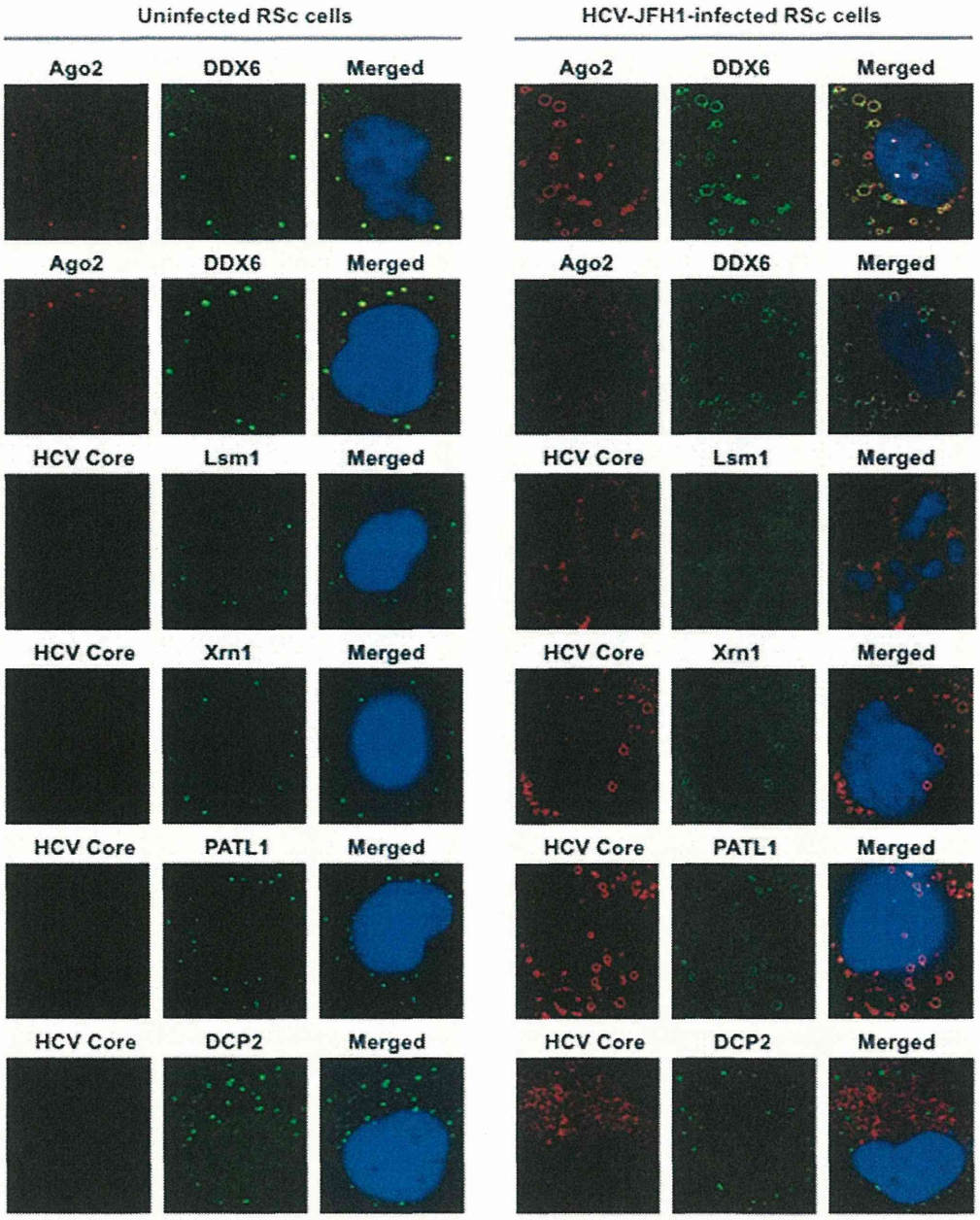

FIG. 2. HCV disrupts the P-body formation of microRNA effectors. Uninfected RSc cells and HCV-JFH1-infected RSc cells at 72 h postinfection were stained with anti-human AGO2 (011-22033) and anti-DDX6 (A300-460A) antibodies. The cells were also stained with anti-HCV core and anti-Lsm1 (LS-C97364), anti-Xrn1 (A300-443A), anti-PATL1, or anti-DCP2 (A302-597A) antibodies and were examined by confocal laser scanning microscopy.

could affect the stress granule formation of G3BP1, ATX2, or PABP1 in response to heat shock or treatment with arsenite. These stress granule components dispersed in the cytoplasm at 37°C, whereas these proteins formed stress granules in response to heat shock at 43°C for 45 min or treatment with 0.5 mM arsenite for 30 min (Fig. 5). In contrast, stress granules were not formed in HCV-JFH1-infected cells at 72 h postinfection in response to heat shock at 43°C for 45 min (Fig. 5), suggesting that HCV-JFH1 infection suppresses stress granule formation in response to heat shock or treatment with arsenite. Intriguingly, G3BP1, ATX2, or PABP1 still colocalized with the HCV core protein even under the above-described stress conditions (Fig. 5). Furthermore, Western blot analysis of cell lysates of uninfected or HCV-JFH1-infected cells at 72 h postinfection showed similar protein expression levels of ATX2, PABP1, HSP70, DDX3, DDX6, and Lsm1 but not G3BP1 (Fig. 6), suggesting that HCV-JFH1 infection does not affect host mRNA translation.

P-body and stress granule components are required for HCV replication. Finally, we investigated the potential role of

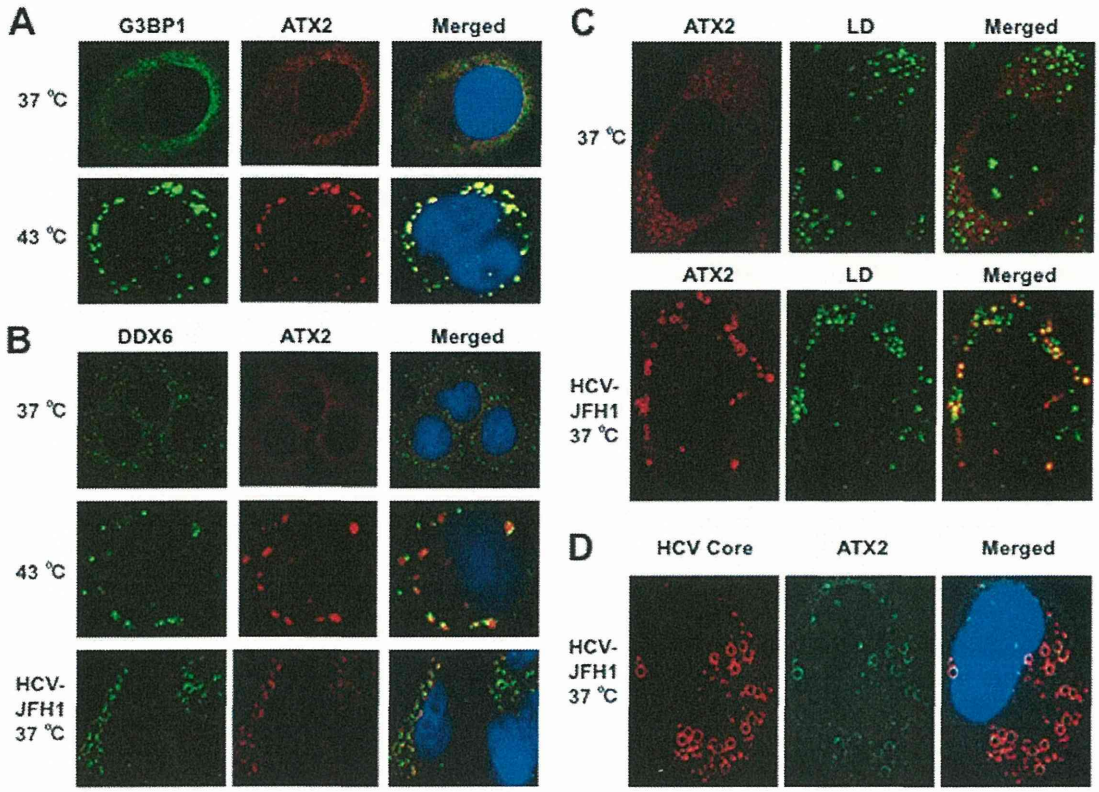

FIG. 3. Dynamic redistribution of ataxin-2 (ATX2) around LDs in response to HCV-JFH1 infection. (A) ATX2 is a stress granule component. RSc cells were incubated at 37°C or 43°C for 45 min. Cells were stained with anti-G3BP1 (A302-033A) and anti-ATX2 (A93520) antibodies and were examined by confocal laser scanning microscopy. (B) Dynamic redistribution of DDX6 and ATX2 in response to heat shock or HCV infection. RSc cells after heat shock at 43°C for 45 min or 72 h after inoculation with HCV-JFH1 were stained with anti-DDX6 and anti-ATX2 (A93520) antibodies. (C) HCV relocalizes ataxin-2 to LDs. HCV-JFH1-infected RSc cells at 72 h postinfection were stained with anti-ATX2 (A93520) antibody and BODIPY 493/503. (D) ATX2 colocalizes with the HCV core protein. HCV-JFH1-infected RSc cells at 72 h postinfection were stained with anti-ATX2/SCA2 (A301-118A) and anti-HCV core antibodies.

P-body and stress granule components in the HCV life cycle. We first used lentiviral vector-mediated RNA interference to stably knock down DDX6 as well as DDX3 in RSc cells. We used puromycin-resistant pooled cells 10 days after lentiviral transduction in all experiments. Real-time LightCycler RT-PCR analysis of DDX3 or DDX6 demonstrated a very effective knockdown of DDX3 or DDX6 in RSc cells transduced with lentiviral vectors expressing the corresponding shRNAs (Fig. 7A). Importantly, shRNAs did not affect cell viabilities (data not shown). We next examined the levels of HCV core and the infectivity of HCV in the culture supernatants as well as the level of intracellular HCV RNA in these knockdown cells 24 h after HCV-JFH1 infection at an MOI of 4. The results showed that the accumulation of HCV RNA was significantly suppressed in DDX3 or DDX6 knockdown cells (Fig. 7B). In this context, the release of the HCV core protein and the infectivity of HCV in the culture supernatants were also significantly suppressed in these knockdown cells (Fig. 7C and D). This finding suggested that DDX6 is required for HCV replication, like DDX3. To further examine the potential role of other P-body and stress granule components in HCV replication, we used RSc cells transiently transfected with a pool of siRNAs specific for ATX2, PABP1, Lsm1, Xrn1, G3BP1, and PATL1 as well as a pool of control siRNAs (siCon) following HCV-JFH1 infection. In spite of the very effective knockdown of each component (Fig. 7E), the siRNAs used in these experiments did not affect cell viabilities (data not shown). Consequently, the accumulation of HCV RNA was significantly suppressed in ATX2, PABP1, or Lsm1 knockdown cells (Fig. 7F), indicting that ATX2, PABP1, and Lsm1 are required for HCV replication. In contrast, the level of HCV RNA was not affected in Xrn1 knockdown cells (Fig. 7F), suggesting that Xrn1 is unrelated to HCV replication. Furthermore, we observed a moderate effect of siG3BP1 and siPATL1 on HCV RNA replication (Fig. 7F). Altogether, HCV seems to hijack the P-body and stress granule components around LDs for HCV replication.

DISCUSSION

So far, the P body and stress granules have been implicated in mRNA translation, RNA silencing, and RNA degradation as well as viral infection (1, 6, 22, 30). Host factors within the P body and stress granules can enhance or limit viral infection, and some viral RNAs and proteins accumulate in the P body and/or stress granules. Indeed, the microRNA effectors DDX6, GW182, Lsm1, and Xrn1 negatively regulate HIV-1 gene expression by preventing the association of viral mRNA

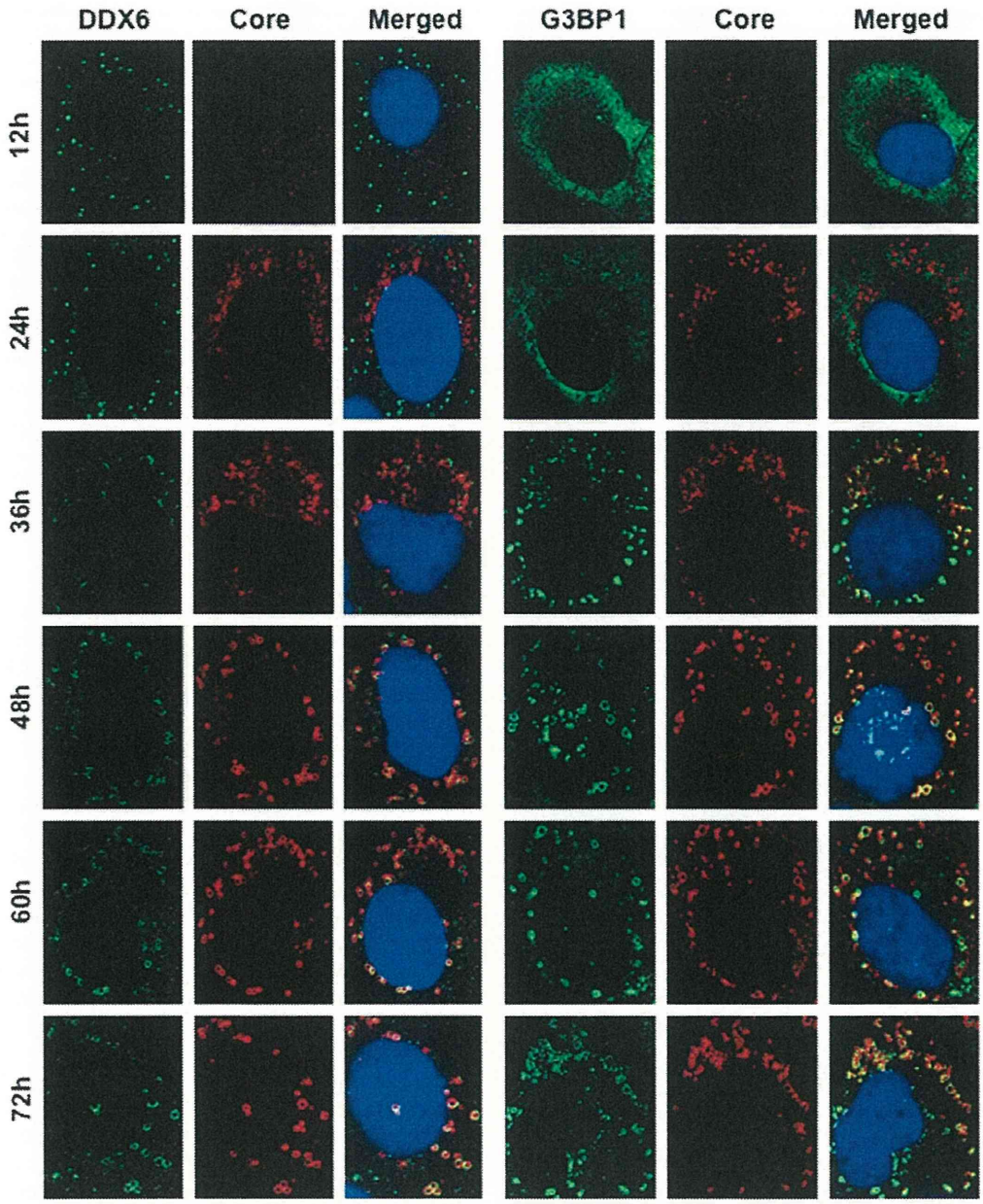

FIG. 4. Dynamic redistribution of DDX6 and G3BP1 in response to HCV-JFH1 infection. RSc cells at the indicated times (hours) after inoculation with HCV-JFH1 were stained with anti-HCV core and either anti-DDX6 (A300-460A) or anti-G3BP1 (A302-033A) antibodies.

with polysomes (9). In contrast, miRNA effectors such as DDX6, Lsm1, PatL1, and Ago2 positively regulate HCV replication (Fig. 7B and F) (16, 31, 33). We have also found that DDX3 and DDX6 are required for HCV RNA replication (3) (Fig. 7B) and that DDX3 colocalized with DDX6 in HCV-JFH1-infected RSc cells (Fig. 1B), suggesting that DDX3 comodulates the DDX6 function in HCV RNA replication. In this regard, the liver-specific miR-122 interacts with the 5′-UTR of the HCV RNA genome and positively regulates HCV replication (15, 17, 19, 20, 31). Since miRNAs usually interact with DDX6 and Ago2 in miRISC and are involved in RNA silencing, DDX6 and Ago2 may be required for miR-122-dependent HCV replication. Indeed, quite recently, a study showed that Ago2 is required for miR-122-dependent HCV RNA replication and translation (40). However, little is known regarding how miR-122 and DDX6 positively regulate HCV replication. Accordingly, we have shown that these miRNA effectors, including DDX6, Lsm1, Xrn1, and Ago2, accumulated around LDs and the HCV production factory and colocalized with the HCV core protein in response to HCV infection (Fig. 1 and 2). However, the decapping enzyme DCP2 did not accumulate and colocalize with the core protein (Fig. 2). Consistent with this finding, Scheller et al. reported previously that the depletion of DCP2 by siRNA did not affect HCV

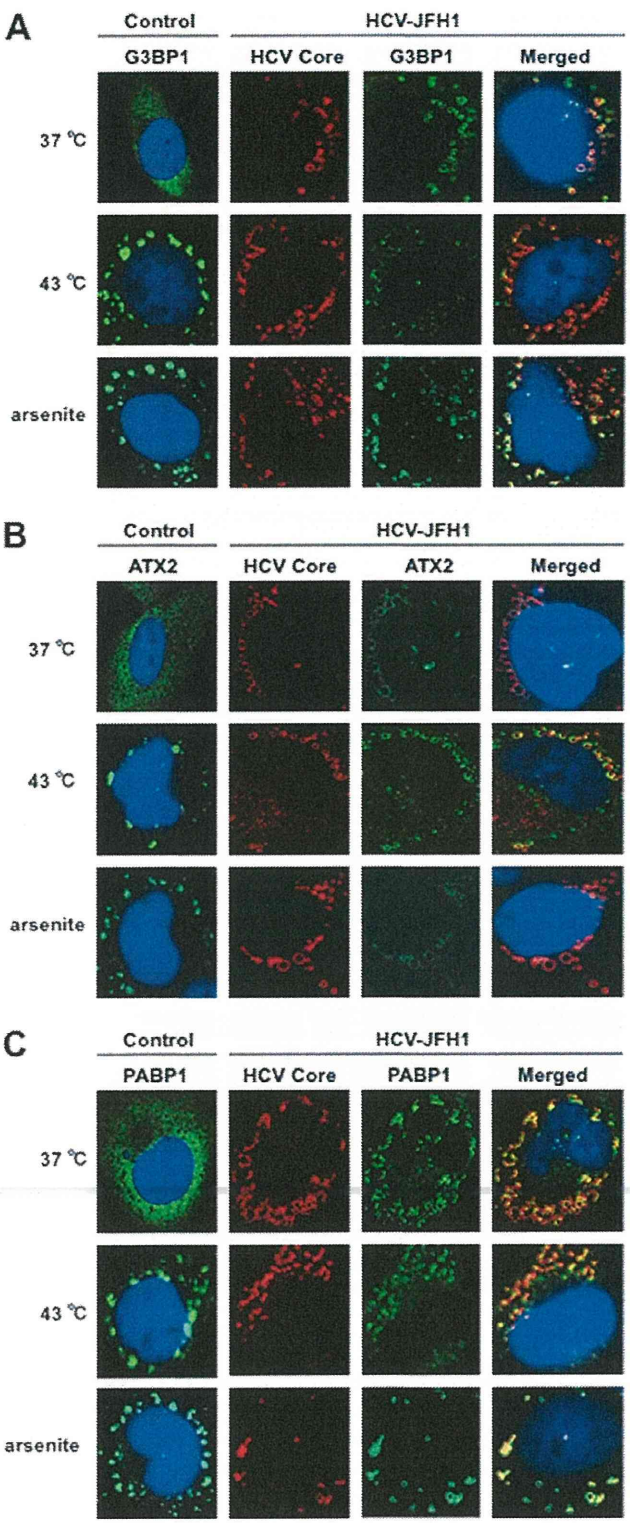

FIG. 5. HCV suppresses stress granule formation in response to heat shock or treatment with arsenite. Naïve RSc cells or HCV-JFH1-infected RSc cells at 72 h postinfection were incubated at 37°C or 43°C for 45 min. Cells were also treated with 0.5 mM arsenite for 30 min. Cells were stained with anti-HCV core and anti-G3BP1 (A), anti-ATX2 (B), or anti-PABP1 (ab21060) (C) antibodies and were examined by confocal laser scanning microscopy.

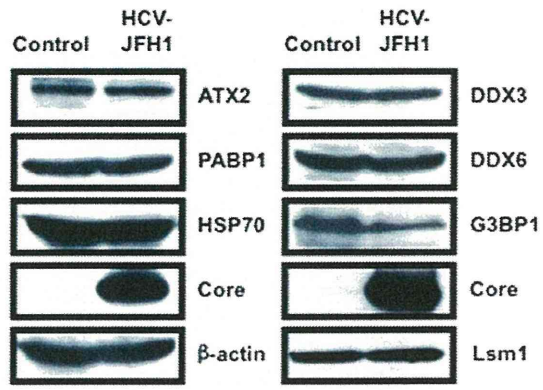

FIG. 6. Host protein expression levels in response to HCV-JFH1 infection. The results of the Western blot analyses of cellular lysates with anti-ATX2/SCA2 antibody (A301-118A), anti-PABP1 (ab21060), anti-HSP70 (610607), anti-HCV core, anti-β-actin, anti-DDX3 (54257 [NT] and 5428 [IN] mixture), anti-DDX6 (A300-460A), anti-G3BP1 (611126), or anti-LSM1 (LS-C97364) antibody in HCV-JFH1-infected RSc cells at 72 h postinfection as well as in naïve RSc cells are shown.

production (33). Since HCV harbors the internal ribosome entry site (IRES) structure in the 5′-UTR of the HCV genome instead of a cap structure, unlike HIV-1, DCP2 may not be recruited on the HCV genome and utilized for HCV replication. Otherwise, DCP2 may determine whether or not DDX6 and miRNAs positively or negatively regulate target mRNA.

Furthermore, we have demonstrated that HCV infection hijacks the P-body and stress granule components around LDs (Fig. 1, 2, 4, and 5). We have found that the P-body formation of DDX6 began to be disrupted at 36 h postinfection (Fig. 4). Consistently, G3BP1 formed stress granules at 36 h postinfection. We then observed the ringlike formation of DDX6 or G3BP1 and colocalization with the HCV core protein after 48 h postinfection, suggesting that the disruption of P-body formation and the hijacking of P-body and stress granule components occur at a late step of HCV infection. Furthermore, HCV infection could suppress stress granule formation in response to heat shock or treatment with arsenite (Fig. 5). In this regard, West Nile virus and dengue virus, of the family *Flaviviridae*, interfere with stress granule formation and P-body assembly through interactions with T cell intracellular antigen 1 (TIA-1)/TIAR (11). Moreover, PABP1 and G3BP1, stress granule components, are known to be common viral targets for the inhibition of host mRNA translation (34, 39). In fact, HIV-1 and poliovirus proteases cleave PABP1 and/or G3BP1 and suppress stress granule formation during viral infection (34, 39). On the other hand, HCV infection transiently induced stress granules at 36 h postinfection (Fig. 4) and did not cleave PABP1 (Fig. 6); however, HCV could suppress stress granule formation in response to heat shock or treatment with arsenite through hijacking their components around LDs, the HCV production factory (Fig. 5). Consistently, Jones et al. showed that HCV transiently induces stress granules of enhanced green fluorescent protein (EGFP)-G3BP at 36 h after infection with the cell culture-generated HCV (HCVcc) reporter virus Jc1FLAG2 (p7-nsGluc2A); however, those authors did not show the recruitment of EGFP-G3BP to LDs (18). Although we do not know the exact reason for this apparent discrepancy,

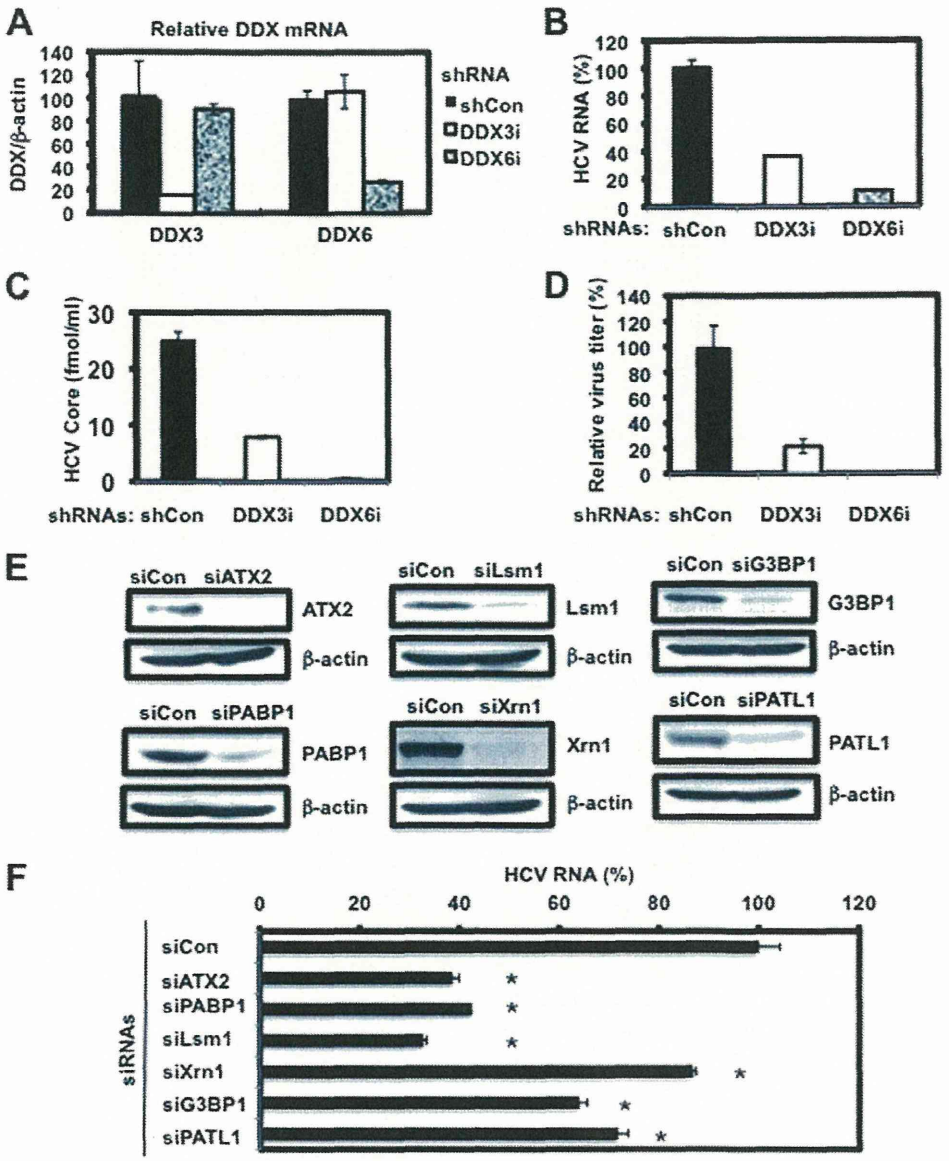

FIG. 7. Requirement of P-body and stress granule components for HCV replication. (A) Inhibition of DDX3 or DDX6 mRNA expression by the shRNA-producing lentiviral vector. Real-time LightCycler RT-PCR for DDX3 or DDX6 was also performed for β-actin mRNA in RSc cells expressing shRNA targeted to DDX3 (DDX3i) or DDX6 (DDX6i) or the control nontargeting shRNA (shCon) in triplicate. Each mRNA level was calculated relative to the level in RSc cells transduced with the control nontargeting lentiviral vector (shCon), which was assigned as 100%. Error bars in this panel and other panels indicate standard deviations. (B) Levels of intracellular genome-length HCV-JFH1 RNA in the cells at 24 h postinfection at an MOI of 4 were monitored by real-time LightCycler RT-PCR. Results from three independent experiments are shown. Each HCV RNA level was calculated relative to the level in RSc cells transduced with a control lentiviral vector (shCon), which was assigned as 100%. (C) The levels of HCV core in the culture supernatants from the stable knockdown RSc cells 24 h after inoculation of HCV-JFH1 at an MOI of 4 were determined by ELISA. Experiments were done in triplicate, and columns represent the mean core protein levels. (D) The infectivity of HCV in the culture supernatants from stable-knockdown RSc cells 24 h after inoculation of HCV-JFH1 at an MOI of 4 was determined by a focus-forming assay at 24 h postinfection. Experiments were done in triplicate, and each virus titer was calculated relative to the level in RSc cells transduced with a control lentiviral vector (shCon), which was assigned as 100%. (E) Inhibition of ATX2, PABP1, Lsm1, Xrn1, G3BP1, or PATL1 protein expression by 72 h after transient transfection of RSc cells with a pool of control nontargeting siRNA (siCon) or a pool of siRNAs specific for ATX2, PABP1, Lsm1, Xrn1, G3BP1, or PATL1 (25 nM), respectively. The results of Western blot analyses of cellular lysates with anti-ATX2, anti-PABP1, anti-Lsm1, anti-Xrn1, anti-G3BP1, anti-PATL1, or anti-β-actin antibody are shown. (F) Levels of intracellular genome-length HCV-JFH1 RNA in the cells at 48 h postinfection at an MOI of 1 were monitored by real-time LightCycler RT-PCR. RSc cells were transiently transfected with a pool of control siRNA (siCon) or a pool of siRNAs specific for ATX2, PABP1, Lsm1, Xrn1, G3BP1, and PATL1 (25 nM). At 48 h after transfection, the cells were inoculated with HCV-JFH1 at an MOI of 1 and incubated for 2 h. The culture medium was then changed and incubated for 22 h. Experiments were done in triplicate, and each HCV RNA level was calculated relative to the level in RSc cells transfected with a control siRNA (siCon), which was assigned as 100%. Asterisks indicate significant differences compared to the control treatment (*, $P < 0.01$).

several possible explanations can be offered. First, those authors examined the localization of EGFP-G3BP within 48 h postinfection, and we observed it at later times (Fig. 4). Second, they used only EGFP-tagged G3BP instead of endogenous G3BP1. Third, they used a Jc1FLAG2 (p7-nsGluc2A) clone, and an HCV-JFH1 clone could markedly induce the recruitment of the core protein to LDs compared to that of Jc1. Also, Jangra et al. failed to observe the recruitment of DDX6 to LDs at 2 days after infection with HJ3-5 virus (16). Accordingly, we also observed that most of the DDX6 still formed intact P bodies at earlier times (12 h or 24 h postinfection). Importantly, we observed the recruitment of DDX6 to LDs 48 h later (Fig. 4). Furthermore, those authors did not show the ringlike structure formation of the HJ3-5 core protein around LDs, unlike the JFH1 core protein that we used in this study. The interaction of the HCV core protein with DDX6 may explain the recruitment of P-body components to LDs. However, we do not yet know whether the P-body function(s) can be performed on LDs. At least, HCV infection did not affect the translation of several host mRNAs with 5′ caps and 3′ poly(A) tails despite the disruption of P-body formation at 72 h postinfection (Fig. 6), suggesting that HCV does not affect P-body function and that HCV recruits functional P bodies to LDs.

We need to address the potential role of stress granule components, such as PABP1, in HCV replication/translation, since the HCV genome does not harbor the 3′ poly(A) tail. Intriguingly, we have found that the accumulation of HCV RNA was significantly suppressed in PABP1 knockdown RSc cells (Fig. 7F). In this regard, Tingting et al. demonstrated previously that G3BP1 and PABP1 as well as DDX1 were identified as the HCV 3′-UTR RNA-binding proteins by proteomic analysis and that G3BP1 was required for HCV RNA replication (35). Yi et al. also reported that G3BP1 was associated with HCV NS5B and that G3BP1 was required for HCV RNA replication (42). We observed a moderate effect of siG3BP1 on HCV RNA replication (Fig. 7F). In contrast, the accumulation of HCV RNA was significantly suppressed in ATX2 and Lsm1 knockdown cells as well as in PABP1 knockdown cells (Fig. 7F), suggesting that ATX2, Lsm1, and PABP1 are required for HCV replication.

Taking these results together, this study has demonstrated for the first time that HCV hijacks P-body and stress granule components around LDs. This hijacking may regulate HCV RNA replication and translation. Indeed, we have found that the accumulation of genome-length HCV-O (genotype 1b) (14) RNA was markedly suppressed in DDX6 knockdown O cells (data not shown). More importantly, these P-body and stress granule components may be involved in the maintenance of the HCV RNA genome without 5′ cap and 3′ poly(A) tail structures in the cytoplasm for long periods, since the hijacking of P-body and stress granule components by HCV occurred at later times.

ACKNOWLEDGMENTS

We thank D. Trono for the lentiviral vector system, T. Wakita for HCV-JFH1, and K. T. Jeang for pHA-DDX3. We also thank T. Nakamura and K. Takeshita for their technical assistance.

This work was supported by a grant-in-aid for scientific research (C) from the Japan Society for the Promotion of Science (JSPS); by a grant-in-aid for research on hepatitis from the Ministry of Health, Labor, and Welfare of Japan; and by the Viral Hepatitis Research Foundation of Japan. M.K. was supported by a research fellowship from the JSPS for young scientists.

REFERENCES

1. **Anderson, P., and N. Kedersha.** 2007. Stress granules: the Tao of RNA triage. Trends Biochem. Sci. **33**:141–150.
2. **Ariumi, Y., et al.** 2003. Distinct nuclear body components, PML and SMRT, regulate the *trans*-acting function of HTLV-1 Tax oncoprotein. Oncogene **22**:1611–1619.
3. **Ariumi, Y., et al.** 2007. DDX3 DEAD-box RNA helicase is required for hepatitis C virus RNA replication. J. Virol. **81**:13922–13926.
4. **Ariumi, Y., et al.** 2008. The DNA damage sensors ataxia-telangiectasia mutated kinase and checkpoint kinase 2 are required for hepatitis C virus RNA replication. J. Virol. **82**:9639–9646.
5. **Ariumi, Y., et al.** 2011. The ESCRT system is required for hepatitis C virus production. PLoS One **6**:e14517.
6. **Beckham, C. J., and R. Parker.** 2008. P bodies, stress granules, and viral life cycles. Cell Host Microbe **3**:206–212.
7. **Bridge, A. J., S. Pebernard, A. Ducraux, A. L. Nicoulaz, and R. Iggo.** 2003. Induction of an interferon response by RNAi vectors in mammalian cells. Nat. Genet. **34**:263–264.
8. **Brummelkamp, T. R., R. Bernard, and R. Agami.** 2002. A system for stable expression of short interfering RNAs in mammalian cells. Science **296**:550–553.
9. **Chable-Bessia, C., et al.** 2009. Suppression of HIV-1 replication by microRNA effectors. Retrovirology **6**:26.
10. **Cristea, I. M., et al.** 2010. Host factors associated with the Sindbis virus RNA-dependent RNA polymerase: role for G3BP1 and G3BP2 in virus replication. J. Virol. **84**:6720–6732.
11. **Emara, M. M., and M. A. Brinton.** 2007. Interaction of TIA-1/TIAR with West Nile and dengue virus products in infected cells interferes with stress granule formation and processing body assembly. Proc. Natl. Acad. Sci. U. S. A. **104**:9041–9046.
12. **Hijikata, M., N. Kato, Y. Ootsuyama, M. Nakagawa, and K. Shimotohno.** 1991. Gene mapping of the putative structural region of the hepatitis C virus genome by in vitro processing analysis. Proc. Natl. Acad. Sci. U. S. A. **88**:5547–5551.
13. **Hijikata, M., et al.** 1993. Proteolytic processing and membrane association of putative nonstructural proteins of hepatitis C virus. Proc. Natl. Acad. Sci. U. S. A. **90**:10773–10777.
14. **Ikeda, M., et al.** 2005. Efficient replication of a full-length hepatitis C virus genome, strain O, in cell culture, and development of a luciferase reporter system. Biochem. Biophys. Res. Commun. **329**:1350–1359.
15. **Jangra, R. K., M. Yi, and S. M. Lemon.** 2010. Regulation of hepatitis C virus translation and infectious virus production by the microRNA miR-122. J. Virol. **84**:6615–6625.
16. **Jangra, R. K., M. Yi, and S. M. Lemon.** 2010. DDX6 (Rck/p54) is required for efficient hepatitis C virus replication but not IRES-directed translation. J. Virol. **84**:6810–6824.
17. **Ji, H., et al.** 2008. MicroRNA-122 stimulates translation of hepatitis C virus RNA. EMBO J. **27**:3300–3310.
18. **Jones, C. T., et al.** 2010. Real-time imaging of hepatitis C virus infection using a fluorescent cell-based reporter system. Nat. Biotechnol. **28**:167–171.
19. **Jopling, C. L., M. Yi, A. M. Lancaster, S. M. Lemon, and P. Sarnow.** 2005. Modulation of hepatitis C virus RNA abundance by a liver-specific microRNA. Science **309**:1577–1581.
20. **Jopling, C. L., S. Schütz, and P. Sarnow.** 2008. Position-dependent function for a tandem microRNA miR-122-binding site located in the hepatitis C virus RNA genome. Cell Host Microbe **4**:77–85.
21. **Kato, N., et al.** 1990. Molecular cloning of the human hepatitis C virus genome from Japanese patients with non-A, non-B hepatitis. Proc. Natl. Acad. Sci. U. S. A. **87**:9524–9528.
22. **Kedersha, N., and P. Anderson.** 2007. Mammalian stress granules and processing bodies. Methods Enzymol. **431**:61–81.
23. **Kuroki, M., et al.** 2009. Arsenic trioxide inhibits hepatitis C virus RNA replication through modulation of the glutathione redox system and oxidative stress. J. Virol. **83**:2338–2348.
24. **Kushima, Y., T. Wakita, and M. Hijikata.** 2010. A disulfide-bonded dimer of the core protein of hepatitis C virus is important for virus-like particle production. J. Virol. **84**:9118–9127.
25. **Mamiya, N., and H. J. Worman.** 1999. Hepatitis C virus core protein binds to a DEAD box RNA helicase. J. Biol. Chem. **274**:15751–15756.
26. **Miyanari, Y., et al.** 2007. The lipid droplet is an important organelle for hepatitis C virus production. Nat. Cell Biol. **9**:1089–1097.
27. **Naldini, L., et al.** 1996. In vivo gene delivery and stable transduction of nondividing cells by a lentiviral vector. Science **272**:263–267.
28. **Nonhoff, U., et al.** 2007. Ataxin-2 interacts with the DEAD/H-box RNA helicase DDX6 and interferes with P-bodies and stress granules. Mol. Biol. Cell **18**:1385–1396.
29. **Owsianka, A. M., and A. H. Patel.** 1999. Hepatitis C virus core protein interacts with a human DEAD box protein DDX3. Virology **257**:330–340.

30. **Parker, R., and U. Sheth.** 2007. P bodies and the control of mRNA translation and degradation. Mol. Cell **25:**635–646.
31. **Randall, G., et al.** 2007. Cellular cofactors affecting hepatitis C virus infection and replication. Proc. Natl. Acad. Sci. U. S. A. **104:**12884–12889.
32. **Rocak, S., and P. Linder.** 2004. DEAD-box proteins: the driving forces behind RNA metabolism. Nat. Rev. Mol. Cell Biol. **5:**232–241.
33. **Scheller, N., et al.** 2009. Translation and replication of hepatitis C virus genomic RNA depends on ancient cellular proteins that control mRNA fates. Proc. Natl. Acad. Sci. U. S. A. **106:**13517–13522.
34. **Smith, R. W., and N. K. Gray.** 2010. Poly(A)-binding protein (PABP): a common viral target. Biochem. J. **426:**1–11.
35. **Tingting, P., F. Caiyun, Y. Zhigang, Y. Pengyuan, and Y. Zhenghong.** 2006. Subproteomic analysis of the cellular proteins associated with the 3′ untranslated region of the hepatitis C virus genome in human liver cells. Biochem. Biophys. Res. Commun. **347:**683–691.
36. **Tourrière, H., et al.** 2003. The RasGAP-associated endoribonuclease G3BP assembles stress granules. J. Cell Biol. **160:**823–831.
37. **Wakita, T., et al.** 2005. Production of infectious hepatitis C virus in tissue culture from a cloned viral genome. Nat. Med. **11:**791–796.
38. **Weston, A., and J. Sommerville.** 2006. Xp54 and related (DDX6-like) RNA helicase: roles in messenger RNP assembly, translation regulation and RNA degradation. Nucleic Acids Res. **34:**3082–3094.
39. **White, J. P., A. M. Cardenas, W. E. Marissen, and R. E. Lloyd.** 2007. Inhibition of cytoplasmic mRNA stress granule formation by a viral proteinase. Cell Host Microbe **2:**295–305.
40. **Wilson, J. A., C. Zhang, A. Huys, and C. D. Richardson.** 2011. Human Ago2 is required for efficient miR-122 regulation of HCV RNA accumulation and translation. J. Virol. **85:**2342–2350.
41. **Yedavalli, V. S., C. Neuveut, Y. H. Chi, L. Kleiman, and K. T. Jeang.** 2004. Requirement of DDX3 DAED box RNA helicase for HIV-1 Rev-RRE export function. Cell **119:**381–392.
42. **Yi, Z., et al.** 2006. Subproteomic study of hepatitis C virus replicon reveals Ras-GTPase-activating protein binding protein 1 as potential HCV RC component. Biophys. Biochem. Res. Commun. **350:**174–178.
43. **You, L. R., et al.** 1999. Hepatitis C virus core protein interacts with cellular putative RNA helicase. J. Virol. **73:**2841–2853.
44. **Zufferey, R., D. Nagy, R. J. Mandel, L. Naldini, and D. Trono.** 1997. Multiply attenuated lentiviral vector achieves efficient gene delivery in vivo. Nat. Biotechnol. **15:**871–875.

HUMAN GENE THERAPY CLINICAL DEVELOPMENT 24:1–12 (XXX 2013)

DOI: 10.1089/humc.2013.066

Research Article

Long-Term Elimination of Hepatitis C Virus from Human Hepatocyte Chimeric Mice After Interferon-γ Gene Transfer

Yuki Takahashi,[1,*] Mitsuru Ando,[1,*] Makiya Nishikawa,[1] Nobuhiko Hiraga,[2] Michio Imamura,[2] Kazuaki Chayama,[2] and Yoshinobu Takakura[1]

Abstract

Chronic hepatitis C virus (HCV) infection is a leading cause of cirrhosis, liver failure, and hepatocellular carcinoma. Although the combination therapy employing pegylated interferon (IFN)-α and ribavirin is effective, this treatment is effective in only approximately 50% patients with genotype 1 HCV infection. IFN-γ is a potent anti-HCV agent that exhibits its antiviral action through a receptor distinct from that for IFN-α. Therefore, IFN-γ application might provide an alternative approach to IFN-α-based therapies. However, recombinant IFN-γ protein exhibits a poor pharmacokinetic property, that is, a very short half-life. It is our hypothesis that sustained IFN-γ serum concentrations produced by gene transfer could effectively eliminate HCV *in vivo*. We examined the *in vivo* antiviral activity in human hepatocyte chimeric mice infected with genotype 1b HCV at high HCV RNA titers (10^5–10^7 copies/ml). The human IFN-γ-expressing plasmid vector pCpG-huIFNγ exhibited prolonged transgene expression in mice compared with the plasmid vector pCMV-huIFNγ. Moreover, the gene transfer of pCpG-huIFNγ eliminated HCV from the liver of the chimeric mice for a sustained period. On the contrary, administration of pCMV-huIFNγ could not eliminate HCV. In conclusion, we found that a single pCpG-huIFNγ injection resulted in long-term elimination of HCV RNA in chimeric mice, providing, for the first time, direct evidence that chronic infection with high titer HCV *in vivo* can be treated by sustained IFN-γ treatment.

Introduction

Chronic hepatitis C virus (HCV) infection is a leading cause of cirrhosis, liver failure, and hepatocellular carcinoma (Niederau *et al.*, 1998). At present, the standard treatment for chronic HCV patients is a combination of pegylated interferon (IFN)-α and ribavirin (Manns *et al.*, 2001; Fried *et al.*, 2002). However, approximately only 50% of patients with genotype 1 HCV infection and a high viral load showed a sustained viral response, which is associated with resistance to IFN-α (Hofmann *et al.*, 2005; Chayama and Hayes, 2011). More recently, telaprevir, an HCV protease inhibitor, administered in combination with pegylated IFN and ribavirin has led to high rates of sustained virologic response. However, approximately 30% of patients with HCV genotype 1 infection did not respond to the combination treatment (Sherman *et al.*, 2011). Therefore, extensive efforts have been made to develop novel anti-HCV therapies that work via different mechanisms from that of IFN-α.

In vitro cell culture studies using HCV subgenomic replicon systems have demonstrated that IFN-γ (type II IFN) is a potent cytokine with anti-HCV activities (Cheney *et al.*, 2002; Frese *et al.*, 2002; Windisch *et al.*, 2005). The IFN-γ antiviral effects were stronger and more sustained than those of type I IFNs, such as IFN-α and IFN-β (Cheney *et al.*, 2002). Moreover, IFN-γ biological actions are mediated by a unique signal transduction pathway through cell surface receptors that are distinct from those of type I IFNs. Therefore, IFN-γ application could be an alternative therapeutic strategy for chronic HCV infection to overcome the drawbacks associated with present IFN-α-based therapies.

On the basis of the findings regarding IFN-γ anti-HCV activities, the therapeutic efficacy of IFN-γ was evaluated in chronic HCV patients. However, IFN-γ had little or no therapeutic effect in chronic HCV patients (Saez-Royuela *et al.*, 1991; Soza *et al.*, 2005). Although IFN-γ was repeatedly administered at high doses in these studies, the very short *in vivo* half-life of IFN-γ might have hampered its therapeutic

[1]Department of Biopharmaceutics and Drug Metabolism, Graduate School of Pharmaceutical Sciences, Kyoto University, Kyoto 606-8501, Japan.
[2]Department of Gastroenterology and Metabolism, Programs for Biomedical Research, Graduate School of Biomedical Science, Hiroshima University, Hiroshima 734-8551, Japan.
*These two authors contributed equally to this work.

potential. IFN-γ disappears rapidly from the systemic circulation because it has a half-life ranging from several minutes to several hours after intravenous or intramuscular administration in humans, probably because of its rapid urinary excretion and degradation (Foon *et al.*, 1985; Wills, 1990).

Among the various strategies for manipulating IFN-γ pharmacokinetics, *in vivo* IFN-γ gene transfer could be a useful method if prolonged transgene expression can be achieved. Shin *et al.* (2005) have investigated whether liver-directed IFN-γ gene transfer using viral vectors was effective in reducing serum HCV RNA titers in primates. They did not observe a significant decrease of circulating viral RNA after multiple IFN-γ gene deliveries, and the modest variations in HCV RNA level observed were within the normal fluctuations in the viral load. The IFN-γ mRNA level in the liver after IFN-γ gene transfer was relatively low and rapidly declined with time, probably because of induction of immune responses. We speculated that a limited level and short duration of IFN-γ expression caused by immune responses might be the reason for the poor anti-HCV effect of IFN-γ and that the utilization of a nonviral vector would be effective in overcoming this concern. In our series of studies, we demonstrated that the mouse IFN-γ-expressing plasmid pCpG-muIFNγ produced high serum IFN-γ levels for >80 days after a single administration and produced a significant therapeutic effect in NC/Nga mice, a model for human atopic dermatitis (Hattori *et al.*, 2010). On the basis of these findings, we hypothesized that sustained supplementation of human IFN-γ expressed from the pCpG vector could result in an *in vivo* antiviral effect on genotype 1 HCV.

Repopulation of the liver with human hepatocytes can be induced using immunodeficient urokinase-type plasminogen activator (uPA) mice, and the human hepatocytes in the mice can be used in HCV infection experiments (Mercer *et al.*, 2001). We and other group previously demonstrated that administration of IFN-α and pegylated IFN-α can reduce HCV RNA level in the serum in this model (Inoue *et al.*, 2007; Hiraga *et al.*, 2009; Abe *et al.*, 2011). Here, we investigated the effects of IFN-γ gene transfer on HCV infection using HCV-infected human hepatocyte chimeric mice.

Materials and Methods

Plasmid DNA

The human IFN-γ-expressing plasmid vectors pCpG-huIFNγ and pCMV-huIFNγ (described as phCMVenh/prom-huIFNγ previously) were constructed as described previously (Ando *et al.*, 2012). pCpG-gLuc-encoding *Gaussia* luciferase (GLuc) was constructed by inserting the GLuc cDNA fragment from the pGLuc-Basic vector (New England Biolab, Madison, WI) into pCpG-mcs (InvivoGen, San Diego, CA). The enhanced green fluorescent protein (EGFP)-expressing plasmid vector pEGFP-N1 was purchased from BD Biosciences Clontech (Palo Alto, CA).

Animal treatment

Generation of the immunodeficient uPA$^{+/+}$/SCID$^{+/+}$ mice and transplantation of human hepatocytes were performed as described previously (PhoenixBio Co., Ltd., Higashihiroshima, Japan) (Tateno *et al.*, 2004). All mice received transplants with frozen human hepatocytes obtained from the same donor. All animal protocols were carried out in accordance with the guidelines of the local committee for animal experiments (Hiroshima University and Kyoto University). Infection, extraction of serum samples, and euthanization of mice were performed under ether anesthesia. Mouse serum concentrations of human serum albumin (HSA), correlated with the repopulation index (Tateno *et al.*, 2004), were measured using the Human Albumin ELISA Quantitation Kit (Bethyl Laboratories Inc., Montgomery, TX). The chimeric mice with a high replacement rate with human hepatocytes were used in the present study. Eight weeks after hepatocyte transplantation, mice were received an intravenous injection of 10^5 copies of HCV.

Human serum samples containing a high titer of genotype 1b HCV were obtained from two chronic hepatitis patients (patient-A and patient-B) who had provided written informed consent for their study participation. The study protocol conformed to the ethics guidelines of the 1975 Declaration of Helsinki and was approved by the review committee of Hiroshima University.

In vivo IFN-γ gene transfer in mice and HCV-infected chimeric mice

Gene transfer to mouse liver was performed by the hydrodynamic injection method (Liu *et al.*, 1999), which allows very high transgene expression, especially in the liver. In brief, ICR mice received a rapid injection of 0.11 μg naked plasmid DNA dissolved in 0.08 ml saline/g body weight into the tail vein within 5 sec. CB17/Icr-Prkd^{scid}/CrlCrlj mice received a rapid injection of 0.22 μg naked plasmid DNA dissolved in 0.1 ml saline/g body weight into the tail vein within 5 sec. Chimeric mice received 250 μg naked plasmid DNA dissolved in 0.1 ml saline/g body weight into the tail vein within 5 sec. Transfection efficiency in each chimeric mouse was estimated by measuring the serum level of secretory transgene products, that is, IFN-γ and GLuc, because IFN-γ and GLuc were not detected in untreated chimeric mouse serum and because serum concentration of secretory proteins reflects the transgene expression level in the liver.

Measurement of serum concentrations of IFN-γ, GLuc, and alanine aminotransferase

Mouse sera were collected at indicated times after gene transfer. Human IFN-γ concentrations were determined using a human IFN-γ ELISA kit (Ready-Set-Go! human IFN-γ ELISA; eBioscience, San Diego, CA). To measure serum GLuc activities, serum was mixed with sea pansy luciferase assay buffer (PiccageneDual; Toyo Ink, Tokyo, Japan), and the chemiluminescence was measured in a luminometer. Serum alanine aminotransferase (ALT) level was measured by quantification kit (Transaminase CII test Wako; Wako Pure Chemical, Osaka, Japan).

RNA extraction and amplification

RNA was extracted from serum and liver samples by Sepa Gene RV-R (Sankojunyaku, Tokyo, Japan) and reverse transcribed using a random primer (Takara Bio Inc., Shiga, Japan) and M-MLV reverse transcriptase (ReverTra Ace; Toyobo Co., Osaka, Japan). Nested polymerase chain reaction (PCR) and quantitation of HCV by Light Cycler (Roche Diagnostic, Tokyo, Japan) were performed as previously reported

(Tateno *et al.*, 2004; Kimura *et al.*, 2008). The lower detection limits were 10^2 copies/ml for nested PCR and 10^3 copies/ml for real-time PCR.

Fluorescence analysis and histopathological analysis of mouse liver

Mouse livers were excised 1 day after gene transfer with pEGFP-N1, placed in Tissue-Tek OCT embedding compound (Sakura Finetechnical Co., Ltd., Tokyo, Japan), and frozen in liquid nitrogen. Frozen liver sections (8 μm thick) were obtained using a cryostat (Jung CM 3000; Leica Microsystems AG, Wetzlar, Germany). The sections were stained with HSA-specific antibody to visualize human hepatocytes. Liver sections were fixed with 4% paraformaldehyde in phosphate-buffered saline (PBS). After blocking with 20% fetal bovine serum in PBS, the liver sections were incubated with polyclonal goat antibody against HSA (1:100 dilution). After washing, Alexa Fluor 568 antigoat secondary antibody (1:500 dilution; Molecular Probes, Invitrogen, Carlsbad, CA) was added, and the stained sections were observed using a confocal laser microscope (A1R MP; Nikon Instruments, Tokyo, Japan). Liver samples obtained from pCpG-huIFNγ-injected mice were examined either by hematoxylin–eosin staining or by immunohistochemical staining with anti-HSA antibody as previously described (Hiraga *et al.*, 2007).

Statistical analysis

Differences were evaluated by the Student's *t*-test, and $p < 0.05$ was considered statistically significant. The pharmacokinetic parameters, area under the serum concentration–time curve (AUC), and mean residence time were calculated for each animal by integration to the endpoint of the experiment (Yamaoka *et al.*, 1978).

Results

IFN-γ expressed by pCpG-huIFNγ shows antiviral activity in HCV subgenomic replicon cells

In vitro IFN-γ anti-HCV activity was evaluated using LucNeo#2 cells. Supplementary Fig. S1A (Supplementary Data are available online at www.liebertpub.com/humc) shows the effect of recombinant IFN-γ protein at different concentrations for 1 or 3 days on luciferase activity in LucNeo#2 cells. A dose- and time-dependent inhibitory effect was observed. On the basis of these results, the antiviral activity of IFN-γ expressed after transfection with pCpG-huIFNγ was examined. A significant inhibitory effect was observed after transfection, and a higher inhibition was observed at 3 days (Supplementary Fig. S1B). IFN-γ levels in the culture medium were 2.9×10^5 and 3.3×10^6 pg/ml, corresponding to approximately 700 and 7,800 IU/ml 1 and 3 days after transfection, respectively (Supplementary Fig. S1C). IFN-γ was not detected in the culture supernatant from non-transfected cells.

Hydrodynamic pCpG-huIFNγ and pCMV-huIFNγ injection results in sustained and transient transgene expression of human IFN-γ, respectively

In our previous studies, we demonstrated sustained expression of murine IFN-γ from pCpG-muIFNγ, a CpG-depleted plasmid vector, in mice after hydrodynamic injection, while transient expression of murine IFN-γ was observed after hydrodynamic injection of pCMV-muIFNγ, a conventional CpG-replete vector (Hattori *et al.*, 2010). To confirm prolonged and transient transgene expression of human IFN-γ from the same types of plasmid vectors, serum IFN-γ concentrations were measured in ICR mice using the hydrodynamic-based method. The serum human IFN-γ concentration was very high in the initial phase and was maintained for up to approximately 240 days after a single hydrodynamic injection (Fig. 1A), while pCMV-huIFNγ failed to show any sustained gene expression. A similar prolonged profile of human IFN-γ was observed in immunodeficient mice for up to 10 days after gene transfer with pCpG-huIFNγ, while the transient profile of serum human IFN-γ concentration was observed after pCMV-huIFNγ injection (Fig. 1B).

Hydrodynamic plasmid DNA injection results in transgene expression in the livers of human hepatocyte chimeric mice

To examine whether *in vivo* gene transfer in the chimeric mice is possible, we conducted an experiment using plasmid DNA encoding GFP to visualize transgene expression in chimeric mouse livers with a high replacement index of human hepatocytes. GFP expression was observed in human hepatocytes, which was confirmed by HSA-specific immunofluorescent staining (Fig. 1C–E). It was found that approximately 1–2% of human hepatocytes were positive for GFP (Supplementary Fig. S2).

A limited antiviral effect can be obtained in chimeric mice infected with genotype 1b HCV after a single injection of pCMV-huIFNγ

To analyze the antiviral effect of IFN-γ gene transfer *in vivo*, chimeric mice with high HCV RNA titers (10^5–10^7 copies/ml) 9–12 weeks after HCV inoculation received gene transfer of pCMV-huIFNγ. We measured the HCV RNA titer (upper panel), HSA concentration (middle panel), and IFN-γ concentration (lower panel) in serum after a single injection of plasmid vector (Fig. 2A–D). In a mouse with serum HCV titer of approximately 1×10^6 copies/ml, the HCV RNA level in serum decreased, but not to zero (Fig. 2A). HCV RNA was also detected in the liver of this mouse by nested PCR (Fig. 2E). In other mice with high HCV titer ($> 4 \times 10^6$ copies/ml), serum HCV titers fell slightly 1 week after gene transfer, but the serum HCV titer rebounded later (Fig. 2B and C). In a mouse that showed low serum IFN-γ concentration after the plasmid DNA administration, serum HCV RNA titer did not decrease (Fig. 2D). These results imply that anti-HCV effect observed in the present study is mediated by IFN-γ.

A marked antiviral effect can be obtained in chimeric mice infected with genotype 1b HCV after a single injection of pCpG-huIFNγ

To investigate whether more sustained supplementation of IFN-γ has a more effective antiviral effect in chimeric mice infected with HCV, pCpG-huIFNγ was administered to HCV-infected human liver chimeric mice. As expected, more sustained IFN-γ expression was observed in each chimeric mouse compared with that seen after the administration of

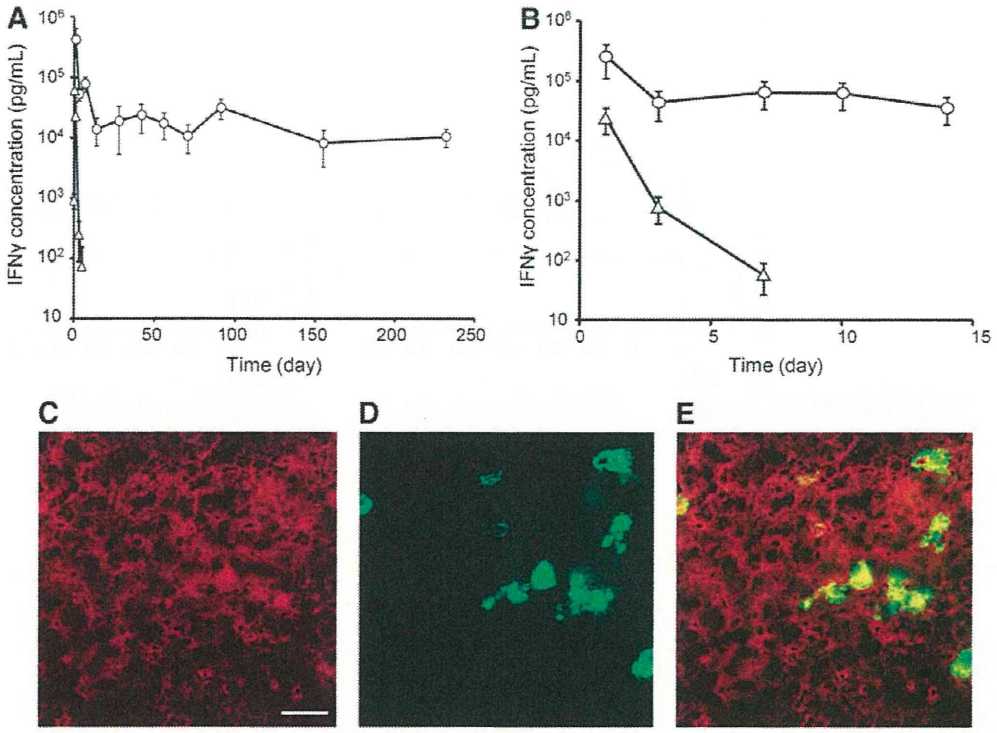

FIG. 1. Prolonged serum concentration of human IFN-γ after hydrodynamic injection of pCpG-huIFNγ and transgene expression in human hepatocytes of the chimeric mice after hydrodynamic administration of plasmid DNA. **(A** and **B)** Plasmid DNA was hydrodynamically injected into mice. **(A)** Four-week-old male ICR mice (normal mice) received an injection of 0.11 μg of pCpG-huIFNγ (circle) or pCMV-huIFNγ (triangle). **(B)** Six-week-old female CB17/Icr-Prkdc^{scid}/CrlCrlj mice (immunodeficient mice) received an injection of 0.22 μg pCpG-huIFNγ (circle) or pCMV-huIFNγ (triangle). Each result represents the mean ± SD of three mice. **(C–E)** Human hepatocyte chimeric mice were injected with 250 μg of plasmid DNA encoding EGFP. One day after gene transfer, the liver was collected and the liver sections were stained with HSA-specific antibody. Typical images of sections exhibiting red fluorescence **(C**; HSA), green fluorescence **(D**; EGFP), and green and red fluorescence **(E**; merged image) are shown. Scale bar = 50 μm. HSA, human serum albumin; IFN, interferon. Color images available online at www.liebertpub.com/humc

pCMV-huIFN-γ, although the absolute IFN-γ levels varied to a great extent. Immediately after pCpG-huIFNγ injection (day 3), HCV RNA levels in the pCpG-huIFNγ-treated mice fell dramatically in 5 of the 6 infected mice (Fig. 3A–E). In a mouse that expressed very low human IFN-γ levels (Fig. 3F), serum HCV titers barely changed after gene transfer with pCpG-huIFNγ. Prolonged undetectable HCV serum levels were observed for more than 7 weeks after gene transfer in all of the surviving mice ($n = 3$) that expressed relatively high human IFN-γ levels. HCV was probably eliminated because no HCV RNA was detected by nested PCR in the livers of the three mice (Fig. 3G). pCpG #4 and pCpG #5 died at 14 and 16 weeks (2 and 4 weeks after IFN-γ gene transfer, respectively) (Fig. 3D and E), although a significant reduction in HCV titers after IFN-γ gene transfer was observed in both mice. These results are summarized in Table 1.

The HCV RNA level in serum was not affected in chimeric mice infected with genotype 1b HCV after a single injection of GLuc-expressing plasmid DNA

Figure 4 shows the results after a hydrodynamic injection of a control vector, pCpG-gLuc, that expresses a reporter protein without any biological activity. Significant GLuc expression was observed in all HCV-infected chimeric mice after *in vivo* gene transfer with pCpG-gLuc. Serum HCV RNA levels did not change in the chimeric mice injected with the control vector, which clearly indicates that the antiviral effect observed in the pCpG-huIFNγ-treated mice was caused by IFN-γ expression and not by hydrodynamic plasmid DNA injection. After hydrodynamic plasmid DNA injection, the HSA levels were hardly affected in any of the mice irrespective of the transgenes encoded by plasmid DNAs.

No apparent damage was observed in hepatocytes of chimeric mice after sustained gene expression of IFN-γ

To evaluate hepatic toxicity induced by IFN-γ, serum ALT was measured before and after hydrodynamic injection of pCpG-huIFNγ. As shown in Fig. 5, serum ALT activity increased at 3–7 days after the administration, but it returned to the level comparable to that before the administration later. As it was found that serum ALT increased at 3 days after the administration of pCpG-huIFNγ, livers were collected at 3 days after the plasmid DNA administration. The liver sections were subjected to hematoxylin eosin staining or to HSA-specific immunohistochemical staining. No obvious damage was observed in the chimeric mouse liver compared with the HCV-infected mouse left untreated (Fig. 6A–D).

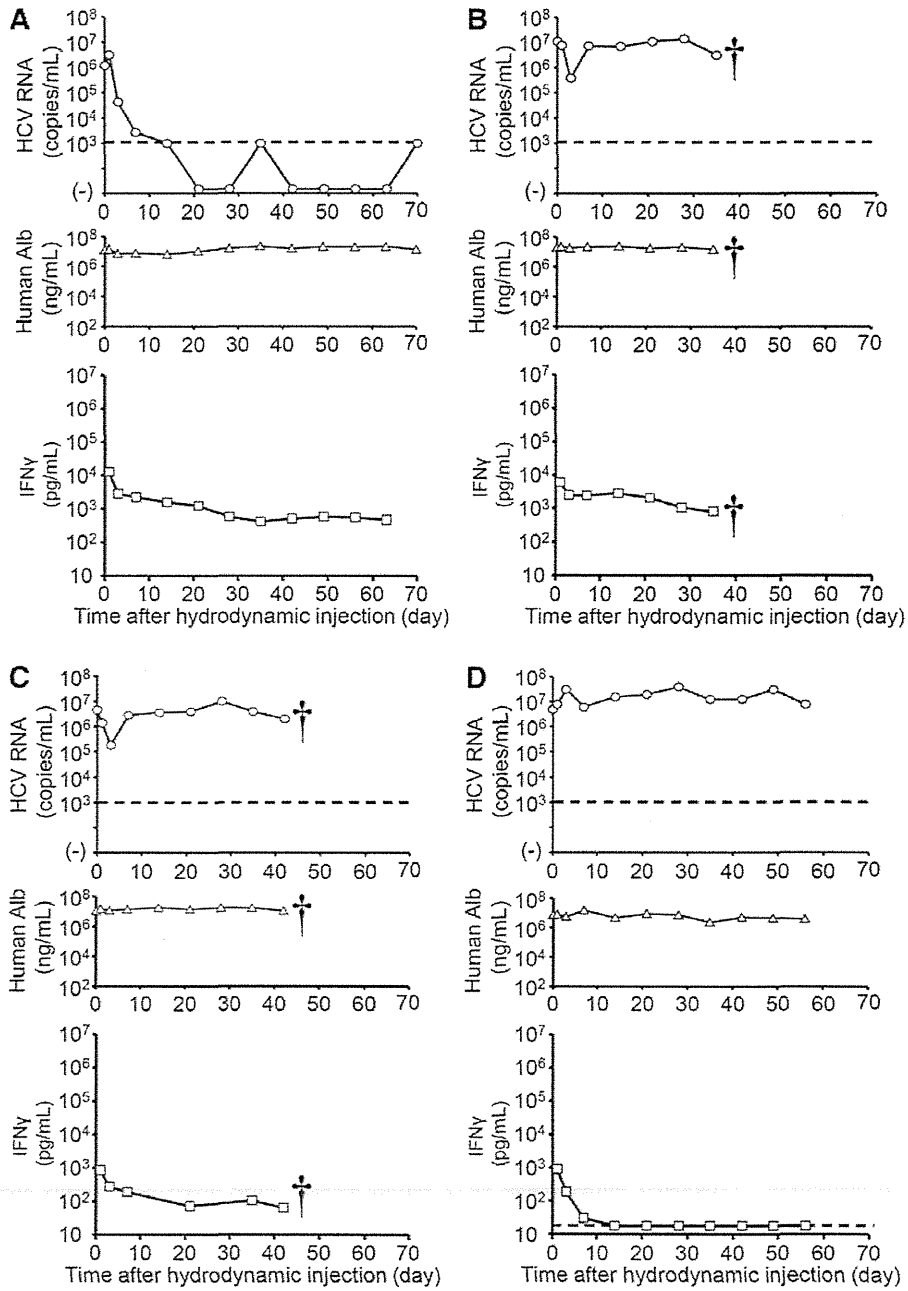

FIG. 2. Effects of intravenous injection of pCMV-huIFNγ in HCV 1b-infected mice. **(A–D)** Mice that had been injected with HCV-positive human serum from patient-A received 250 μg of pCMV-huIFNγ. Panels **(A–D)** correspond to pCMV #1–4, respectively. Serum concentration of HCV RNA copy number (○), HSA (△) and IFN-γ (□) is shown. The horizontal dashed line represents the detection limit (10^3 copies/ml for HCV RNA and 18 pg/ml for IFN-γ). "(-)" on the vertical axis indicates negative for HCV by nested PCR. Dagger (†) indicates the time at which the mice died. **(E)** Nested PCR in pCMV-huIFNγ-treated mouse livers (lane 2: pCMV #1). Mouse livers with (lane 1) or without (lane 3) HCV infection were also analyzed as controls. HCV, hepatitis C virus; PCR, polymerase chain reaction.

To further evaluate a possible toxic effect on the liver induced by sustained IFN-γ expression in the liver, livers were collected from the pCpG-huIFNγ-treated chimeric mice or pCpG-gLuc-treated chimeric mice at the end of the experiments. As shown in Fig. 6E–H, no obvious damage was observed in pCpG-huIFNγ-treated chimeric mouse liver compared with the liver of pCpG-gLuc-treated chimeric mice. Moreover, IFN-γ expression resulted in no apparent reduction of mice serum HSA levels (Fig. 3), suggesting that sustained IFN-γ exposure would not induce severe toxicity in the liver.

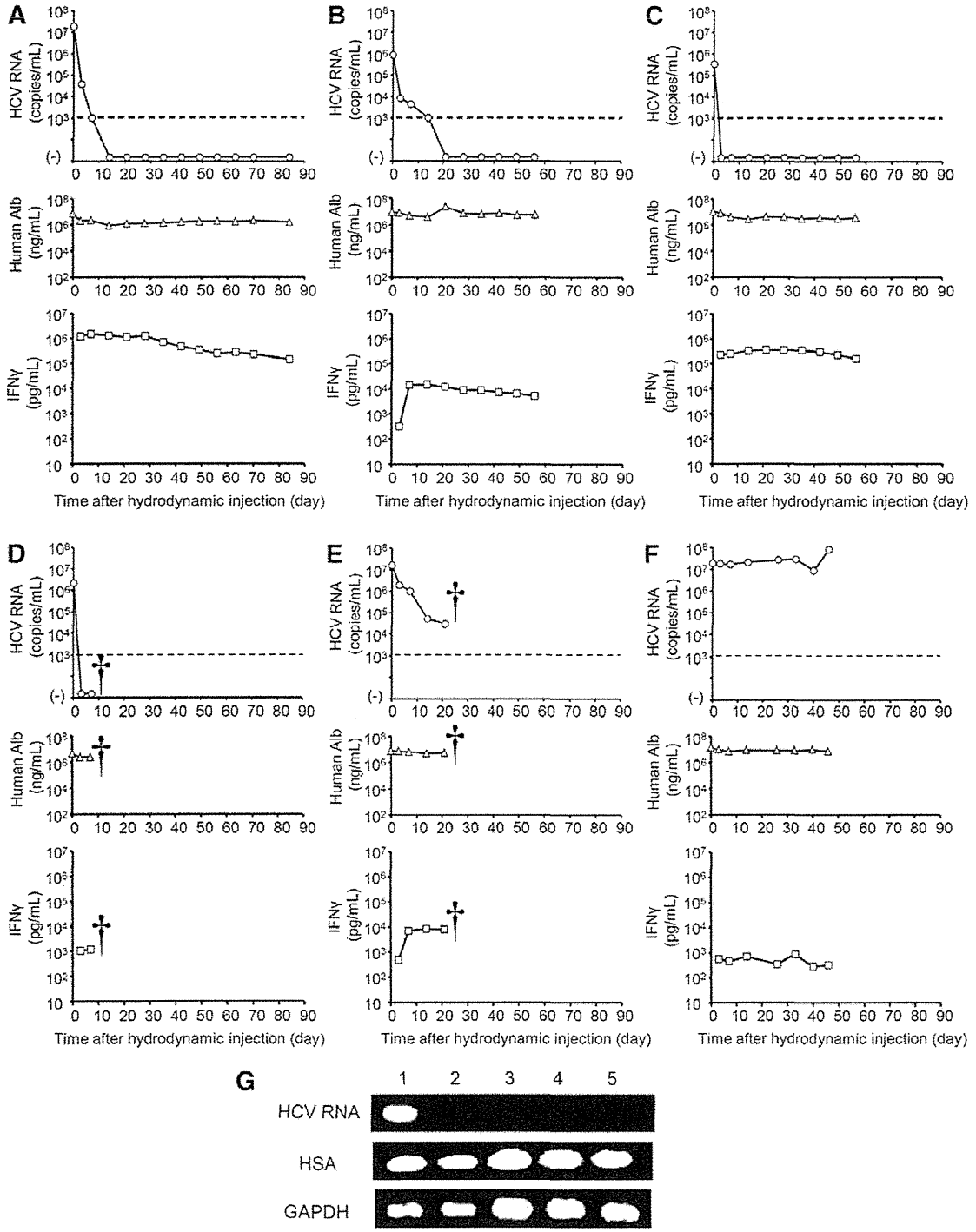

FIG. 3. Effects of intravenous injection of pCpG-huIFNγ in HCV 1b-infected mice. **(A–F)** Mice that had been injected with HCV-positive human serum from either patient-A or patient-B received 250 μg of pCpG-huIFNγ. Panels **(A–F)** correspond to pCpG #1–6, respectively. Serum concentration of HCV RNA copy number (○), HSA (△) and IFN-γ (□) is shown. The horizontal dashed line represents the detection limit (10^3 copies/mL). "(-)" on the vertical axis indicates negative for HCV by nested PCR. Dagger (†) indicates the time at which the mice died. **(G)** Nested PCR in pCpG-huIFNγ-treated mouse livers (lanes 2–4: pCpG #1–3). Mice livers with (lane 1) or without (lane 5) HCV infection were also analyzed as controls.

TABLE 1. SUMMARY OF INTERFERON-γ PHARMACOKINETIC PARAMETERS AND ANTI-HEPATITIS C VIRUS EFFECTS AFTER ADMINISTRATION OF INTERFERON-γ-EXPRESSING PLASMID VECTORS

				IFN-γ pharmacokinetic parameters		
Mouse	*Source*	*HCV RNA at day 0 (copies/ml)*	*Human Alb at day 0 (ng/ml)*	*AUC (pg·day/ml)*	*Mean residence time (day)*	*HCV RNA detection*
pCMV #1	Patient-A	1.2×10^6	1.3×10^7	8.0×10^4	17	±
pCMV #2[a]	Patient-A	1.1×10^7	2.0×10^7	7.5×10^4	14	+
pCMV #3[a]	Patient-A	4.5×10^6	1.1×10^7	6.1×10^3	14	+
pCMV #4	Patient-A	5.0×10^6	7.4×10^6	2.0×10^3	1.8	+
pCpG #1	Patient-A	1.8×10^7	7.6×10^6	5.6×10^7	27	−
pCpG #2	Patient-A	8.8×10^5	9.0×10^6	5.1×10^5	25	−
pCpG #3	Patient-B	3.3×10^5	1.1×10^7	1.6×10^7	27	−
pCpG #4[a]	Patient-A	2.1×10^6	4.6×10^6	6.2×10^3	4.6	−
pCpG #5[a]	Patient-A	1.6×10^7	7.8×10^6	1.3×10^5	13	±
pCpG #6	Patient-A	1.9×10^7	1.5×10^7	1.3×10^4	13	+

pCMV #1–4 correspond to Fig. 2A–D, and pCpG #1–6 correspond to Fig. 3A–F, respectively.
[a]Mouse died before the end of the experiments.
AUC, area under the serum concentration–time curve; HCV, hepatitis C virus; IFN, interferon.

Discussion

Human hepatocyte chimeric mice are useful model animals and have been used in variety of basic experiments involving pharmacological and toxicological investigations associated with drug metabolism by cytochrome P450s (Katoh *et al.*, 2008; Yoshizato and Tateno, 2009; Sanoh *et al.*, 2012) and mechanistic studies of viral infections (Sainz Jr. *et al.*, 2012), as well as in therapeutic approaches to HCV infection (Hiraga *et al.*, 2007; Meuleman *et al.*, 2012). In the present study, we utilized human hepatocyte chimeric mice to test our hypothesis that a sustained IFN-γ supply could be a promising therapeutic option for the treatment of chronic HCV infection.

The present study has demonstrated that a single gene transfer of IFN-γ can result in a significant antiviral effect on human HCV in human hepatocyte chimeric mice with high HCV RNA titers (10^5–10^7 copies/ml). To our knowledge, this is the first report that clearly demonstrates the *in vivo* effectiveness of IFN-γ on a high titer HCV infection model. It was apparent that the anti-HCV effect obtained by pCpG-huIFNγ in this study was significantly greater than that of IFN-γ recombinant protein in the same chimeric mouse model under a similar high HCV burden (Ohira *et al.*, 2009). Anti-HCV effects were observed after repeated administration of recombinant human IFN-γ at high doses (1×10^5 IU on the first day and thereafter 2×10^4 IU/day for 13 days) when the serum HCV RNA titers were $<10^3$ copies/ml. However, when the titers increased ($>10^3$ copies/ml), the preventive effects of recombinant IFN-γ on HCV infection were no longer observed. In the present study, HCV rebound was not observed for up to 8 weeks after a single gene transfer of pCpG-huIFNγ (Fig. 3), and the sustained HCV RNA elimination from the liver was confirmed by nested PCR. As hydrodynamic injection of pCpG-huIFNγ results in IFN-γ transgene expression in the liver, high local concentration of IFN-γ in the liver may be a reason for the strong antiviral effect. Further study is required to determine whether IFN-γ gene delivery into other organs than the liver shows a significant anti-HCV effect.

In the present study, we also tested the anitviral effect of transient IFN-γ expression by using pCMV-huIFNγ. Serum concentration of IFN-γ in the chimeric mice injected with pCMV-huIFNγ was lower and less sustained than that in the mice injected with pCpG-huIFNγ, although IFN-γ expression from pCMV-huIFNγ was more persistent in the chimeric mice compared with that in ICR mice (Fig. 1A). As far as antiviral effect was concerned, only a marginal or no effect was obtained in mice that received pCMV-huIFNγ. It is noteworthy that HCV rebound was observed in the pCMV-huIFNγ-treated mice with reduced HCV titer in serum, suggesting that long-term IFN-γ supplementation is more favorable for preventing HCV rebound.

We have summarized the IFN-γ pharmacokinetics and anti-HCV effects after IFN-γ gene transfer in Table 1. In the case of a high virus titer ($>4\times10^6$ copies/ml serum), a strong antiviral effect was observed in a mouse that showed a high IFN-γ AUC (5.6×10^7 pg·day/ml; pCpG #1) and in a mouse exhibiting a moderate IFN-γ AUC (1.3×10^5 pg·day/ml; pCpG #5). However, little or no antiviral effect was observed in mice with a high virus titer ($>4\times10^6$ copies/ml serum) and a small IFN-γ AUC ($<10^5$ pg·day/ml; pCMV #2–4 and pCpG #6). When the virus titer was relatively low ($<4\times10^6$ copies/ml serum), viral clearance or a strong antiviral effect was observed irrespective of the IFN-γ AUC (pCMV #1, pCpG #2–4). These results indicate that a higher IFN-γ concentration is required to obtain anti-HCV effects in HCV infection with a high titer, while a relatively low IFN-γ concentration is enough to obtain anti-HCV effects in HCV infection with a low titer. In addition to the duration of IFN-γ expression, a transient high concentration of IFN-γ may contribute to a potent antiviral effect, as shown in pCMV #1. We also found that the rate of HCV reduction after IFN-γ was different among mice; that is, the HCV titer in pCpG #3 and #4 decreased more rapidly than that in the other responding mice. Although the detailed mechanism is not clear, there was a tendency that the higher the HCV titer, the slower the response to IFN-γ gene expression, indicating that HCV titer is also an important factor in determining the response of IFN-γ treatment.

SCID mice without functional T and B lymphocytes possess normal NK cell function and elevated hemolytic complement activity and retain their innate immune response